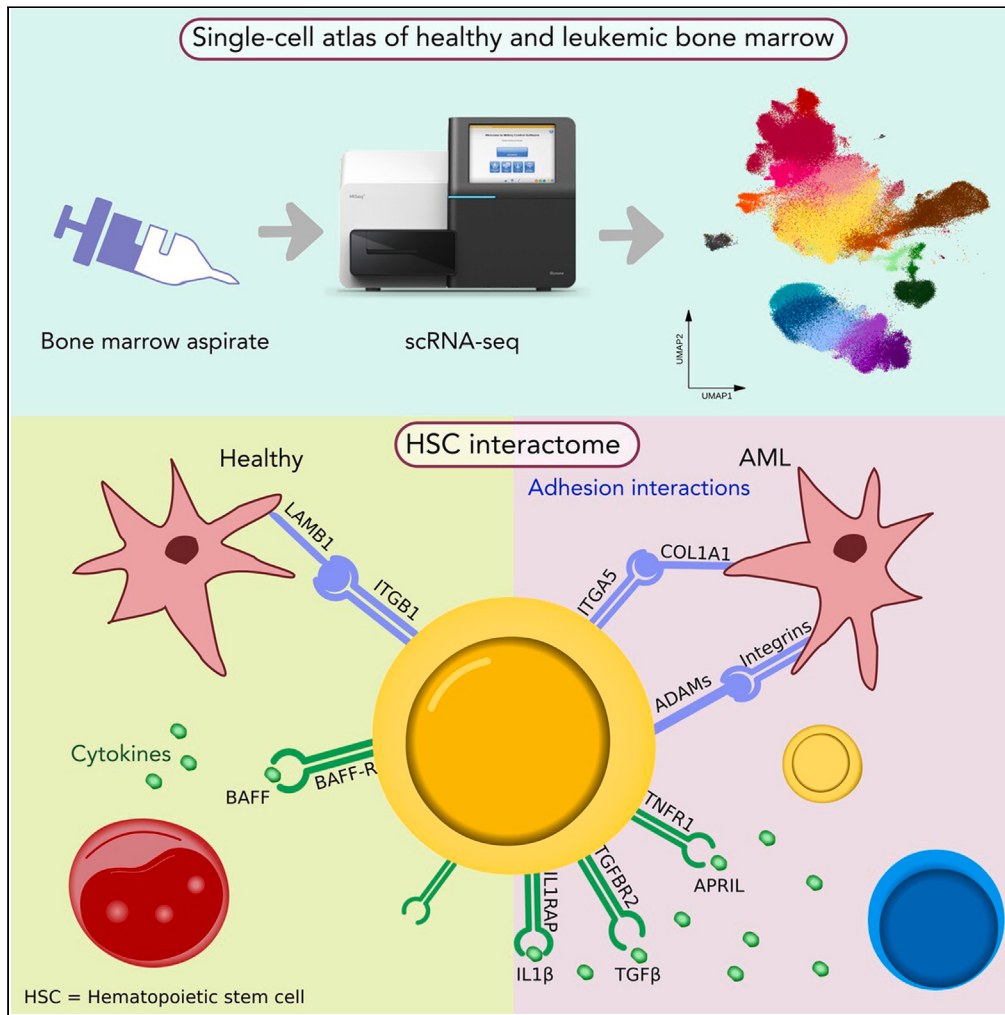


## Article

## Cell-cell interactome of the hematopoietic niche and its changes in acute myeloid leukemia



Sarah Ennis,  
Alessandra  
Conforte, Eimear  
O'Reilly, ...,  
Philippe Krebs,  
Pilib Ó Broin, Eva  
Szegezdi

eva.szegezdi@  
universityofgalway.ie

**Highlights**

Largest atlas of single-cell gene expression in human bone marrow to date

Changes in cell type composition and gene expression in multiple AML cell types

Predicted interactome of hematopoietic stem cells and other bone marrow cell types

Adhesion and cytokine interactions that have potential as therapeutic targets in AML

Ennis et al., iScience 26,  
106943  
June 16, 2023 © 2023 The  
Author(s).  
<https://doi.org/10.1016/j.isci.2023.106943>



## Article

## Cell-cell interactome of the hematopoietic niche and its changes in acute myeloid leukemia

Sarah Ennis,<sup>1,2</sup> Alessandra Conforte,<sup>3</sup> Eimear O'Reilly,<sup>3</sup> Javid Sabour Takanlu,<sup>3</sup> Tatiana Cichocka,<sup>3</sup> Sukhraj Pal Dhami,<sup>3</sup> Pamela Nicholson,<sup>4</sup> Philippe Krebs,<sup>5</sup> Pilib Ó Broin,<sup>1,2,6</sup> and Eva Szegezdi<sup>1,3,6,7,\*</sup>

## SUMMARY

**The bone marrow (BM) is a complex microenvironment, coordinating the production of billions of blood cells every day. Despite its essential role and its relevance to hematopoietic diseases, this environment remains poorly characterized. Here we present a high-resolution characterization of the niche in health and acute myeloid leukemia (AML) by establishing a single-cell gene expression database of 339,381 BM cells. We found significant changes in cell type proportions and gene expression in AML, indicating that the entire niche is disrupted. We then predicted interactions between hematopoietic stem and progenitor cells (HSPCs) and other BM cell types, revealing a remarkable expansion of predicted interactions in AML that promote HSPC-cell adhesion, immunosuppression, and cytokine signaling. In particular, predicted interactions involving transforming growth factor  $\beta$ 1 (TGF $\beta$ 1) become widespread, and we show that this can drive AML cell quiescence *in vitro*. Our results highlight potential mechanisms of enhanced AML-HSPC competitiveness and a skewed microenvironment, fostering AML growth.**

## INTRODUCTION

The hematopoietic niche within the human bone marrow (BM) consists of a diverse range of hematopoietic and nonhematopoietic (such as endothelial, mesenchymal, and osteolineage) cells.<sup>1</sup> The role of the niche is to regulate hemostasis by coordinating the homing, self-renewal, proliferation, and differentiation of hematopoietic stem and progenitor cells (HSPCs) and orchestrate the daily production of myeloid, lymphoid, and erythroid lineage blood cells. This environment is tightly regulated through reciprocal interactions between HSPCs and the niche.<sup>2</sup> For example, C-X-C motif chemokine ligand 12 (CXCL12)-expressing mesenchymal stromal cells play a crucial role in supporting HSPCs by tethering them in the BM via interaction with CXCR4, thus facilitating HSPC quiescence and survival.<sup>3,4</sup> These regulatory interactions are known to be disrupted in leukemia, where the malignant cells alter the niche to support their proliferation and survival. At the same time, these changes make the microenvironment less hospitable to normal HSPCs, leading to their egress and impaired blood cell production.<sup>5</sup>

This is also the case in acute myeloid leukemia (AML), an aggressive blood cancer characterized by rapid accumulation of myeloid lineage precursor cells in the BM. Mouse models of AML have shown that the BM-engrafting AML cells gradually erode the stroma leading to an over 90% non-erythroid stromal cell loss in advanced disease.<sup>6</sup> This skewed microenvironment is known to drive drug resistance and consequent relapse,<sup>7</sup> but the mechanisms and the responsible cellular interactions are not well understood.<sup>8</sup> Better characterization of the cell-cell interactions in the BM and how they change in AML may provide opportunities for a “two-pronged” treatment approach by directly targeting the cancer cells with chemotherapy while also disrupting their interactions with the microenvironment so that it becomes inhospitable to malignant cells.

Advancements in technology, such as improved mouse models and the development of single-cell and spatial transcriptomics have increased our understanding of the biology of the normal hematopoietic niche, particularly in mice.<sup>9,10</sup> However, a large-scale characterization of the composition and behavior of the niche in humans and its perturbation in malignancy is lacking. Although single-cell RNA-sequencing (scRNA-seq) has been applied to the study of the BM and has provided valuable insights,<sup>9–18</sup> due to economic and experimental hurdles, most of these studies have remained restricted to mouse models or cells

<sup>1</sup>The SFI Centre for Research Training in Genomics Data Science, Galway, Ireland

<sup>2</sup>Discipline of Bioinformatics, School of Mathematical & Statistical Sciences, University of Galway, H91 TK33 Galway, Ireland

<sup>3</sup>Apoptosis Research Centre, School of Biological & Chemical Sciences, University of Galway, H91 TK33 Galway, Ireland

<sup>4</sup>Next Generation Sequencing Platform, University of Bern, Bern, Switzerland

<sup>5</sup>Institute of Tissue Medicine and Pathology, University of Bern, Bern, Switzerland

<sup>6</sup>These authors contributed equally

<sup>7</sup>Lead contact

\*Correspondence: [eva.szegezdi@universityofgalway.ie](mailto:eva.szegezdi@universityofgalway.ie)

<https://doi.org/10.1016/j.isci.2023.106943>



**Table 1. Summary of datasets included in this study**

Dataset no.	Healthy donors	AML donors	No. of samples	No. of cells	Reference
1	0	10	28	111,347	Current study
2	3	0	4	20,344	Granja et al. <sup>12</sup>
3	20	0	25	69,264	Oetjen et al. <sup>13</sup>
4	4	5	9	100,407	Petti et al. <sup>14</sup>
5	5	16	41	38,019	van Galen et al. <sup>15</sup>
<b>Total</b>	<b>32</b>	<b>31</b>	<b>107</b>	<b>339,381</b>	

from few donors. Also, as these experiments are typically performed on BM aspirates, cells that are more adherent, such as BM stromal cells (BMSCs) are underrepresented.<sup>19</sup> Another challenge when using scRNA-seq to characterize the leukemic BM is the very high degree of heterogeneity between patients. Because these studies typically only include tens of patients, it is difficult to identify unifying mechanisms of leukemogenesis, allowing only patient-level analysis.<sup>14–16</sup>

Here we report a large-scale analysis of the bone marrow cell-cell interactome in health and upon development of AML. By integrating multiple scRNA-seq datasets generated from BM aspirates (Table 1), a large database has been generated (339,381 cells from 63 donors) that enabled us to identify even rare populations of cells, such as BMSC, and perform a comprehensive analysis of the HSPC interactome in the hematopoietic niche. Using this dataset we established a baseline reference of healthy cells and then identified changes in cell type composition, gene expression, and predicted ligand-receptor interactions of HSPCs that may occur during the development of AML. The results highlight the widespread potential alterations in the BM cellular interactome in AML, especially impacting cell adhesion and cytokine signaling.

## RESULTS

### A harmonized single-cell atlas of healthy and AML BM

To generate a single-cell atlas of the BM in health and AML, we performed droplet-based scRNA-seq on BM aspirates from 10 AML patients collected at key stages of disease progression (diagnosis, post-treatment/remission, and relapse; clinical information available in Table S1) and integrated the data with other openly available scRNA-seq datasets of healthy and AML BM. We identified 4 suitable datasets<sup>12–15</sup> and processed each of them through a uniform pre-processing pipeline to minimize any study-specific effects (Table 1, and further information on each individual sample is provided in Table S2).

To ensure optimal batch correction of the datasets and enable simple reuse and sharing of the atlas, we used scArches<sup>20</sup> (Figure S1) to generate a harmonized reference atlas of the BM. The atlas consists of a total of 339,381 cells from 63 donors (Figure 1). Cell types within the dataset were labeled using a combination of predictive and manual annotations. First, cell type labels were predicted for each cell using the dataset published by Granja and colleagues.<sup>12</sup> We then confirmed the predicted labels and annotated cell types that were not included in the Granja dataset based on expression of well-known marker genes (Figures 1D and 1E). Overall, we identified 19 different cell types including all expected hematopoietic lineage cells, such as HSPCs, and multiple myeloid, lymphoid, and erythroid populations (Figure 1D). Due to the large size of the dataset, we were also able to identify clusters of rare and underrepresented cell types such as BM mesenchymal stromal cells and megakaryocytes which could not be identified in any of the individual datasets prior to integration. The integrated dataset can be downloaded from the Zenodo repository accompanying this publication, along with a Google Colab notebook demonstrating how to explore and reuse it.

### Cell type proportions in the BM are significantly altered during the establishment and progression of AML

To understand the HSPC interactome in the BM, first we determined how its cellular composition changes in health and at different stages of AML progression. We used the propeller function from the speckle R package to test whether there are statistically significant changes in cell type proportions during development and progression of AML.<sup>21</sup> The analysis showed that in healthy BM, over 65% of cells are mature lymphoid lineage cells, around 15% are mature myeloid cells, and the rest are progenitor cells, erythroid, and other rare cell types (Figure 2A). A significant shift in cell type proportions took place at the onset of

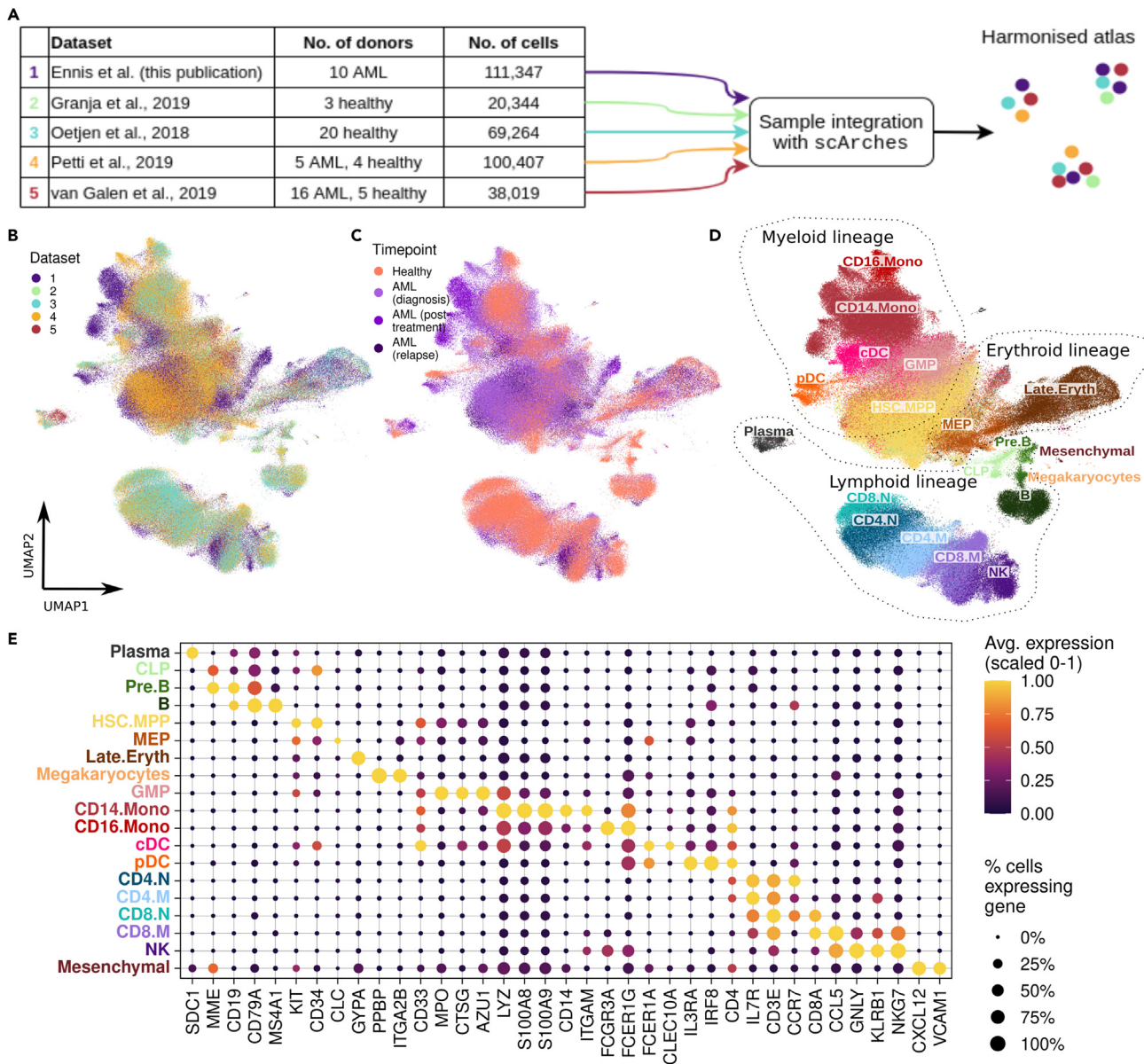


**Figure 1. A harmonised single-cell atlas of healthy and AML BM**

(A) Schema of dataset generation.

(B-D) UMAP was used for dimensionality reduction and visualization of the dataset. Cells are colored by dataset (B), time point (C), and cell type (D).

(E) Dotplot depicting the expression of known marker genes for each identified cell type. The size and color of each dot represent the percentage of cells expressing the gene and the normalized expression level in each cell type, respectively. CD4/8.N, CD4/8 naive T; CD4/8.M, CD4/8 memory T; NK, natural killer cell.

AML with myeloid progenitor cells making up over 50% of BM cells (Figure 2A). In particular, the most primitive myeloid progenitor population, hematopoietic stem cell/multipotent progenitor cells (HSC.MPP), became significantly enriched at diagnosis. Post-treatment, during remission, these proportions returned to levels similar to the healthy condition, but at relapse, as expected, enrichment of myeloid progenitors reappeared (Figure 2B).

In addition to these expected changes, profound changes also took place in the lymphoid lineage. The proportion of common lymphoid progenitors (CLPs) dropped upon development of AML and failed to return to pre-disease levels in remission. The loss of CLP was associated with a profound drop in its progeny,

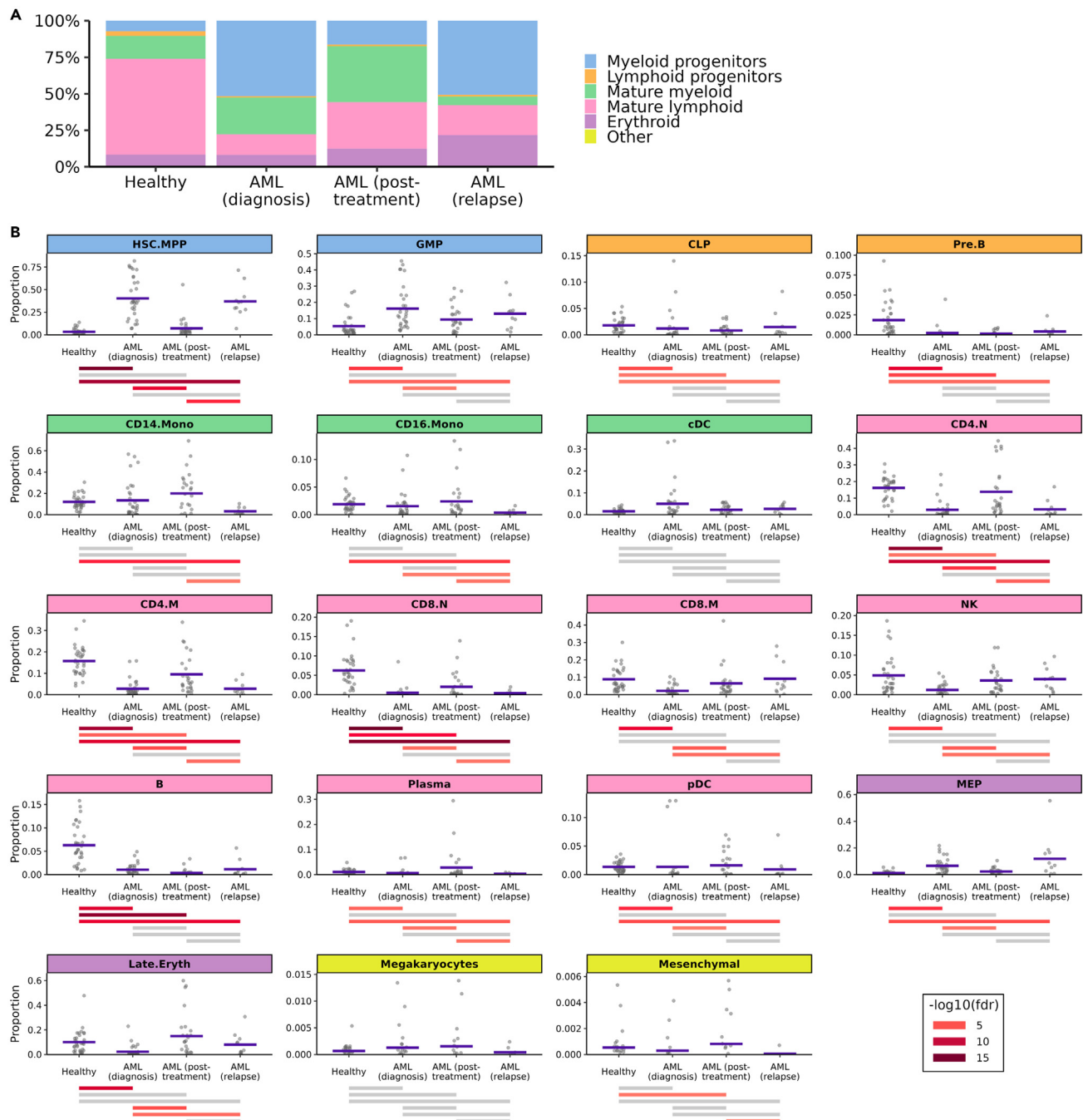


**Figure 2. Cell type proportions in the BM are significantly altered during the establishment and progression of AML**

(A) Percentage of different cell lineages at each time point.

(B) The blue bars show the propeller estimated proportion of each cell type at different time points. The gray dots represent the proportions of each cell type in individual samples. The lines below each plot represent the significance level of the change in proportions between each pair of time points (t-test). Cell types that showed a significant change in proportions between a given pair of time points are represented by colored lines, and gray lines indicate  $FDR \geq 0.05$ . The background color of the facet labels depicts which lineage (as in A) the cell type belongs to. CD4/8.N, CD4/8 naive T; CD4/8.M, CD4/8 memory T; NK, natural killer cell.

especially pre-B cells (Pre.B), mature B cells, and to a lesser extent of CD4<sup>+</sup> and CD8<sup>+</sup> naive T cells (CD4.N, CD8.N) and CD4<sup>+</sup> memory T cells (CD4.M). These results reveal that the adaptive immune system suffers long-term damage either due to the disease or due to the chemotherapy. Corroborating this notion,

B and T cells have been previously reported to display impaired function in AML.<sup>22,23</sup> This impaired function is likely to be exacerbated by their reduced numbers, which may be important to consider with regard to predicting the efficacy of T cell- and B cell-based immunotherapies.<sup>24</sup>

A further indication of impaired immune tumor surveillance in AML was that cytotoxic lymphoid cells (CD8<sup>+</sup> memory T cells [CD8.M] and natural killer [NK] cells) became enriched at relapse, compared to diagnosis, suggesting that although cytotoxic cell numbers recover during remission, they fail to eliminate the leukemic cells or dampen anti-AML immune responses, thus allowing relapse (Figure 2B).<sup>25</sup>

### Impact of AML on gene expression in the BM

Given that the majority of cells in the dataset were from either healthy donors ( $n = 115,445$ ) or AML patients at diagnosis ( $n = 129,626$ ), we decided to focus the remainder of the analysis on these two time points. To uncover functional changes in BM cell types at the onset of AML, we determined changes in gene expression for each cell type upon development of AML. To minimize false discoveries, differentially expressed genes (DEGs) were calculated using a pseudobulk approach, implemented in the Libra R package,<sup>26</sup> and the DEGs were then used as input for gene ontology (GO) enrichment analysis. Most cell types showed broad-scale changes in gene expression, with a median of 2,368 genes being differentially expressed ( $|\text{avg. logFC}| \geq 1$ , adj. p value  $\leq 0.05$ ) (Figure 3A). Of all cell types, pre.B, conventional dendritic cell (cDC), CD4.M, CD14+ monocytes (CD14.Mono), and HSC.MPPs had the highest number of DEGs. Notably, pre.B cells showed downregulation of genes mediating B cell maturation (e.g., VPREB1, TCL1A) and upregulated heat shock protein expression (HSPA1A, HSPA1B), indicating cellular stress (Figure S2). In HSC.MPPs, genes associated with HSPC self-renewal and differentiation (PBX1<sup>27,28</sup>), angiogenesis (VEGFA, NRP1, PDGFA), and myeloid cell differentiation (CSF1R, PTBP3, interleukin [IL] 11) were some of the most notable DEGs (Figure 3C). Importantly, the top upregulated gene in HSC.MPP cells, IL 1 receptor accessory protein (IL1RAP, avg. logFC = 3.79, adj. p value = 1.94e-33), mediates IL-1 $\beta$  signaling, which has been shown to promote the growth and survival of malignant cells in AML and to play a central role in remodeling the BM microenvironment into a niche favoring leukemogenesis over normal hematopoiesis by driving pro-inflammatory signaling.<sup>29</sup>

GO (Biological Process) terms enriched among up- and downregulated genes for each cell type were clustered into groups based on similarity. There were 6 clusters of similar GO terms enriched among downregulated genes and another 6 clusters of GO terms enriched among genes upregulated upon development of AML (Figure 3B and 3C). Three clusters of GO terms enriched among downregulated genes affected most BM-resident cell types. These consisted of processes associated with DNA repair, transcription, and oxidative metabolism (cluster 1); lymphocyte functionality (cluster 3); and oxygen levels (hypoxia), detoxification, and necrotic cell death (cluster 5, Figure 3B). Importantly, the most significantly enriched GO terms among downregulated genes were pathways of mitochondrial respiration (with downregulation of several genes of the mitochondrial electron transport chain: NDUFA4, UQCRC, COX6B1). This was detectable in all BM-constituent cell types, except HSC.MPP, megakaryocyte erythrocyte precursor (MEP), and megakaryocytes, revealing widespread hypoxia and metabolic reprogramming of nearly all non-malignant BM cell types. Downregulation of genes associated with cell division was also present in multiple cell types but mostly affected CLP and pre.B cells (cluster 2). CLP and pre.B cells also displayed impaired mRNA transportation and protein maturation, signs of proteostatic cellular stress (cluster 4, Figure 3B).

The first group of processes upregulated in AML centered on morphogenesis and cytokine signaling (cluster 1) predominantly affecting pre.B cells, the malignant population-encompassing HSC.MPP, MEP and granulocyte monocyte precursor (GMP) populations, and plasmacytoid dendritic cells (pDCs). Of note, there was little overlap in the specific GO terms across these cell types. For example, the enriched pathways for MEPs and GMPs differed from each other (e.g., "regulation of IL-6 production" was enriched among genes upregulated in MEPs but not GMPs).

The second cluster of processes enriched among upregulated genes involved the phosphatidylinositol 3-kinase (PI3K) and signal transducer and activator of transcription (STAT) pathways, especially in CLP and pre.B, where these pathways drive cell proliferation and cell survival before and after immunoglobulin (Ig) heavy chain and light chain recombination, during which the cells are non-proliferative.<sup>30</sup> Downregulation of mitotic activity (cluster 2 of downregulated pathways) and simultaneous induction of proliferative signaling in these cell cohorts indicate deregulation of B cell receptor assembly (via Ig-recombination) and thus early B cell maturation in AML.



**Figure 3. Impact of AML on gene expression in the BM**

For each cell type, DEGs were identified by comparing gene expression in AML diagnostic samples to healthy samples.

(A) Volcano plots showing number of DEGs for each cell type.

(B–C) GO terms enriched among genes significantly down- (B) and upregulated (C) in AML. All significantly enriched GO terms are on the vertical axis, and the pink heatmap shows the adj. p value for the enrichment of each term in each cell type (hypergeometric test). The white/purple matrix represents the similarity between GO terms with clusters of similar terms highlighted with colored boxes. The word clouds beside each cluster show the keywords enriched in that cluster of terms.

(D) Enrichment of terms related to metabolism and respiration among genes downregulated in AML. CD4/8.N, CD4/8 naive T; CD4/8.M, CD4/8 memory T; NK, natural killer cell.

The largest cluster of GO terms enriched among upregulated genes (cluster 3) was made up of processes related to T cell differentiation, where CLP, Pre.B, HSC.MPP, and pDC cells showed upregulation of genes that drive helper T cell differentiation (IL6R, IL18). This indicates that the leukemic microenvironment may skew lymphoid progenitor maturation toward T cell generation over B cells and may partially explain the

significant B cell depletion observed at all AML time points compared to healthy samples (Figure 2B). Other clusters of terms enriched among upregulated genes (clusters 4 & 5) particularly affected HSC.MPPs and were related to transforming growth factor  $\beta$  (TGF- $\beta$ ) signaling and cell adhesion pathways.

### Interactions between HSPCs and their niche

Cell-cell interactions are central in regulating the hematopoietic BM niche and HSPC maintenance. The role of the niche in controlling HSPC self-renewal, expansion, and differentiation are well recognized. There is also accumulating evidence that during development of AML, cell-cell interactions change substantially. To gain a comprehensive understanding of HSPC-niche communication pathways and how they change upon development of AML, we predicted ligand-receptor interactions between HSC.MPP and all other BM-resident cell types by looking at the expression of genes that code for ligands and their interacting receptors using the liana R package.<sup>31</sup> A combination of interaction prediction methods was run using the OmniPath database of known ligand-receptor interactions,<sup>32</sup> which generated a list of high-confidence, well-curated interactions in healthy BM and upon development of AML. This list of interactions is available to explore and download via an interactive web app ([https://sarahennis.shinyapps.io/HSC\\_Interactome/](https://sarahennis.shinyapps.io/HSC_Interactome/)), along with plots showing the expression of the ligand and receptor genes in the interacting cell types.

A total of 485 and 905 potential interactions were predicted in healthy and AML diagnostic samples, respectively (Figure 4A). Of the total 1,390 interactions, only 354 were common to both time points, demonstrating the extent of the impact that leukemia has on the interactome of hematopoietic cells (Figure 4A). Of the interactions that were common to both time points, 34 had a higher interaction score in healthy samples, 43 had a higher score in AML, and 277 remained unchanged (Figure S3A, Table S5). Notably, AML-HSC.MPPs could participate in a large number of interactions which were not predicted in healthy BM and involved all BM-constituent cell types (Figure 4A). This may not be because leukemic HSC.MPPs expressed a higher range of ligands and receptors in comparison to normal HSC.MPPs; instead, it likely reflects the intra-patient heterogeneity of AML where different AML sub-populations co-exist in individual patients and form varied, partially overlapping interactions.

The predicted interactions also varied on a broad scale with regards to how specific they were to given cell types (Figure 4C). We have identified 13 ubiquitous predicted interactions (Figure 4D), where the interacting partner of the HSC.MPP-expressed ligand or receptor was present in at least 14 other cell types (over 75% of BM-constituent cell types). On the other end of the scale, 159 interactions were cell type specific; i.e., the partner ligand or receptor was only present in one cell type (Figures 4E–4G). The number of HSC.MPP-interacting cells for the remaining interactions varied but showed trends where cell types within each hematopoietic cell lineage tended to participate in similar interactions.

The ubiquitous predicted interactions were dominated by cell-adhesion mediators, involving integrin beta-1 (ITGB1), galectins (LGALS1, LGALS9, LGALS3BP), and CD44. Additionally, angiopoietin-1 (ANGPT1) and TGF- $\beta$ 1 (TGFB1) signaling was detected (Figure 4D). There was a pronounced shift in these ubiquitous interactions upon development of AML. Firstly, in AML, ITGB1 was predicted to form interactions with a broader spectrum of ligands, including the disintegrin and metalloprotease family members, ADAM-15 and -17, as well as the growth factor, angiopoietin-1 (ANGPT1). In addition to enabling adhesion, these interactions could allow HSC.MPPs to receive pro-survival signals from nearly all BM cell types.<sup>33</sup> Another striking change was in the TGFB1-TGFB receptor-2 (TGFB2R) interaction, which was predicted to be widespread in AML, with CD14.mono cells being a major interacting partner. TGFB1 is a pleiotropic regulator of all stages of hematopoiesis, and excessive TGFB1 expression has been linked to proliferation of leukemic cells and failure of normal hematopoiesis in chronic lymphocytic leukemia.<sup>34</sup> In AML, TGFB1 has been linked to leukemia stem cell/leukemia-initiating cell quiescence<sup>4</sup> as well as BM fibrosis,<sup>35</sup> however, how TGF- $\beta$ 1 signaling changes upon AML and the role of CD14 monocytes in the process have not been understood.

The opposite trend was seen for the interaction between amyloid precursor protein (APP) and the plasma membrane molecular chaperone, CD74, which was widespread in healthy BM but was not predicted in AML. CD74 mediates trafficking of APP into endocytotic vacuoles thus preventing the production of amyloid- $\beta$  peptide, the main constituent of senile plaques in Alzheimer's disease.<sup>36</sup> Loss of the interaction in AML was due to significant downregulation of CD74 expression, which occurred in 13 out of the 19 BM cell types. Loss of CD74 expression may contribute to enhanced fitness of leukemic HSC.MPPs as CD74 has been reported to regulate HSPC maintenance and its deficiency in mice caused accumulation of

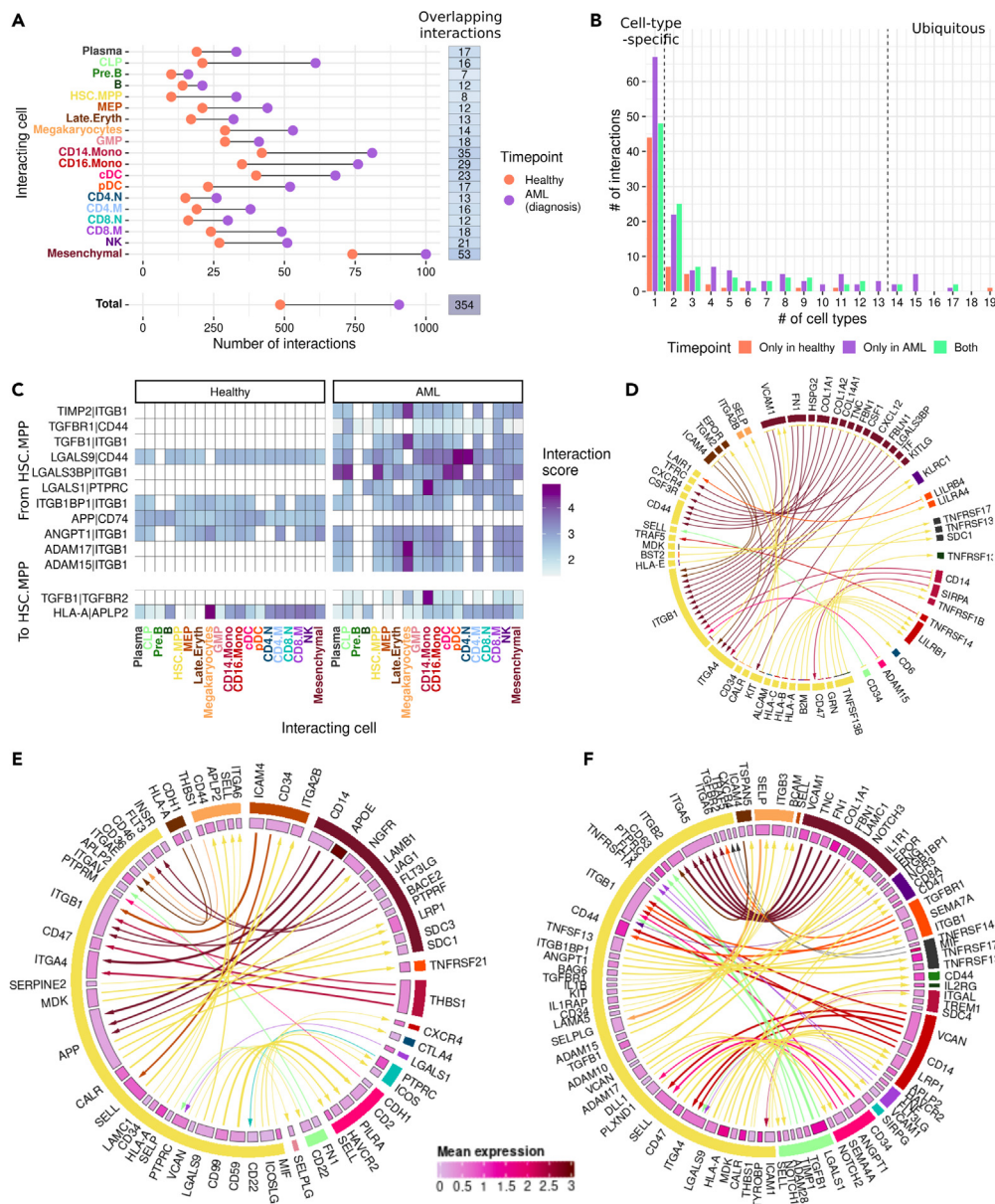


**Figure 4. Predicted interactions between HSPCs and their niche**

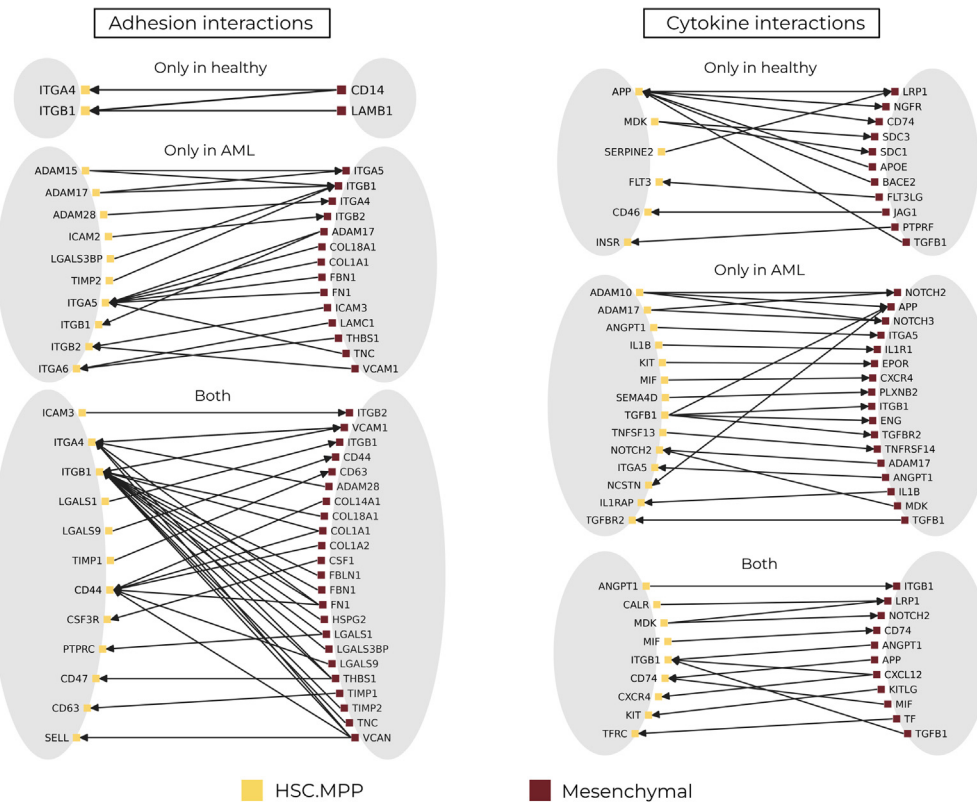
(A) Ligand-receptor interactions predicted between HSC.MPP cells and the other cell types in healthy and AML BM.

(B) Histogram showing the number of cell types each interaction was identified in.

(C) Genes and cell types involved in ubiquitous interactions ( $\geq 14$  cell types).

(D-F) Chord diagrams of cell-type-specific interactions identified at both time points (D) or exclusively in healthy (E) or diagnostic (F) samples. The color of the outer sectors represents cell type (colors same as in A), and links are colored by cell type of the sending cell. In E-F the inner sectors represent the mean expression of the ligand/receptor gene and the width of links is proportional to the interaction score. CD4/8.N, CD4/8 naive T; CD4/8.M, CD4/8 memory T; NK, natural killer cell.

HSPCs in the BM due to their increased potential to compete for BM niches.<sup>37</sup> Alternatively, as a major histocompatibility complex (MHC)-II chaperone, reduced CD74 expression may play an immunosuppressive role, causing reduced MHC-II complex expression, affecting antigen presentation and thus enabling immune escape.<sup>38</sup>

**Figure 5. Predicted interactions between HSCs and BM mesenchymal cells**

Predicted interactions were grouped into those involved in cell adhesion and those involved in cytokine signaling.

With regards to the most active HSC.MPP-interacting cell types, a similar pattern can be seen in healthy and AML BM—bone marrow mesenchymal stromal cell (BMSC) cells were predicted to form the highest number of interactions with HSC.MPPs, followed by  $CD14^+$  and  $CD16^+$  monocytes (CD14.Mono, CD16.Mono) (Figure 4B). These cell types are known to play important roles in regulating the hematopoietic niche, particularly BMSC, which are essential for HSPC maintenance.<sup>2,39</sup> The top 50% of predicted interactions between HSC.MPP cells and BMSC and monocytes in healthy BM vs. AML are shown in Figure S4.

### The HSPC and BMSC interactome

Since BMSCs are key regulators of HSPC maintenance, ranging from HSPC quiescence, proliferation, homing, and migration to survival, detailed analysis of the BMSC-HSC.MPP interactome was carried out. Both healthy and AML-HSC.MPPs were predicted to form broad-scale interactions facilitating cell-cell and cell-extracellular matrix (ECM) adhesion with adhesion molecules and ECM components expressed by BMSCs (Figure 5). Potential interactions of the adhesion receptors, ITGA4, ITGB1 (forming the very late antigen [VLA]-4 complex), and CD44 of HSC.MPPs with collagens, fibronectin, laminins, and other BMSC-produced ECM components as well as the cell-cell adhesion ligands VCAM1, VCAN, and galectins (LGALS1, LGALS3BP) expressed on the surface of BMSCs were detectable, facilitating HSC.MPP engraftment in the niche. Reciprocally, HSC.MPPs also expressed adhesion ligands, such as galectins (LGALS1, LGALS9), ICAM3, and TIMP1 that could bind to adhesion receptors of BMSCs (CD44, ITGB1, ITGB2, CD63). All these interactions were unchanged, predicted both in healthy BM and in AML.

In AML, however, a number of additional cell-ECM and cell-cell adhesion interactions were predicted. AML-HSC.MPPs showed increased expression of ITGA5 (avg. logFC = 2.1, adj. p val = 6.42e-14) enabling VLA-5 assembly (ITGA5-ITGB1 complex) and induction of ITGA6 (avg. logFC = 1.04, adj. p value = 1.16e-4) as well as of adhesion ligands, most notably members of the ADAM family (ADAM-15, -17). This could

enable the formation of further adhesion interactions with ECM proteins (via ITGA5, ITGA6) and BMSC-expressed adhesion proteins (VCAM1 and VCAN via ITGB2), revealing that engraftment of AML-HSC.MPPs in the hematopoietic niche remains essential or it is strongly beneficial to AML cells. Of note, the recognized leukemic stem cell markers ITGA5 and ITGA6<sup>40</sup> were predicted to form interactions with fibronectin (FN) and tenascin C (TNC), with TNC being important for hematopoiesis and known to co-distribute with FN and collagen III surrounding HSPCs.<sup>33,41</sup> The expansion of potential adhesion interactions in AML is likely to increase the competitiveness of AML-HSC.MPPs to engraft in protective niches that provide pro-survival signals and may also contribute to chemoresistance.

In addition to cell-matrix and cell-cell adhesion, BMSCs and HSC.MPPs could engage in a large number of cell-cell and cytokine-cell communication interactions (Figure 5). Many well-established interactions between HSC.MPPs and BMSCs were detected, including CXCL12-CXCR4, KITLG-KIT (Kit ligand and its receptor), and CSF-CSF3R (colony stimulating factor-3/G-CSF and its receptor). In addition, several novel interactions HSC.MPPs formed with BMSCs were also predicted. For example, interactions between MIF (macrophage migration inhibitory factor), a pleiotropic cytokine regulating innate immunity, and one of its receptors, CD74; CALR and LRP1 (calreticulin and low-density lipoprotein related protein 1); and MDK (midkine) and two receptors (LRP1 and NOTCH2) were predicted both in healthy and AML BM. The MIF-CD74 interaction was reciprocal, where both HSC.MPPs and BMSCs expressed both the ligand and the receptor, creating a signaling circuitry driving ERK (extracellular signal-regulated kinase) and PI3K signaling.<sup>42</sup>

MDK is a heparin-binding growth factor that can bind to multiple receptors and mediates anti-apoptotic, mitogenic, and chemotactic signaling. The interactome analysis found that HSC.MPP-expressed MDK interactions with LRP1 and NOTCH2 were stable, while interactions with syndecan 1 (SDC1) and 3 were lost upon development of AML. On the other hand, a reciprocal interaction was predicted in AML, where BMSC-expressed MDK could bind NOTCH2 on HSC.MPPs, potentiating NOTCH2 signaling in HSC.MPPs. In addition to MDK, AML-BMSCs induced expression of ADAM17 which can also interact with NOTCH2 facilitating its proteolytic processing and activation. AML-HSC.MPPs thus experience higher NOTCH2 signaling, which has been shown to reduce myeloid differentiation and enhance long- and short-term HSPC repopulation upon stress hematopoiesis.<sup>43</sup> NOTCH signaling was affected not only in HSC.MPPs but also in AML-BMSCs. ADAM10, -15, and -17 expressed by AML-HSC.MPPs were predicted to form interactions with NOTCH2 and NOTCH3 expressed by BMSCs driving NOTCH2/3-activation, which has been shown to block BMSC differentiation and osteogenesis and may enhance BM-mediated drug resistance.<sup>44,45</sup>

In the AML-BM, a number of interactions that were not present in healthy BM were predicted. Firstly, IL1B (IL-1 $\beta$ ) produced by HSC.MPPs and BMSCs could activate inflammatory signaling via binding to IL1R1 (IL1 receptor 1) on BMSCs and IL1RAP (IL1 receptor associated protein 1) on HSC.MPPs. Notably, IL-1 $\beta$  levels are fine-tuned in the BM, and chronic IL-1 $\beta$  exposure has been shown to restrict HSPC lineage output and to weaken healthy HSPC self-renewal capacity.<sup>46</sup> IL-1 $\beta$  also promotes AML blast proliferation by induction of growth factors and cytokines, like CSF3.<sup>47</sup>

Finally, an interaction between the semaphorin family member, SEMA4D, expressed by HSC.MPPs and its receptor, PLXNB2, on BMSCs was predicted in AML. SEMA4D is known to inhibit osteoblast differentiation in multiple myeloma patients, where bone resorption is abundant. This process may be aggravated by TGFB1 signaling, which also became enhanced in AML, with both HSC.MPPs and BMSCs expressing TGFB1 which could activate TGFBR2 on the other cell type. While the effects of TGFB1 on BMSCs are multifold and not fully understood, TGFB1 has been shown to reduce osteoblastic differentiation and facilitate the development of a myelodysplastic syndrome (MDS)/AML-like BMSC phenotype.<sup>48</sup>

### Altered cell adhesion and cytokine signaling in AML

To determine how the predicted interactions regulate cell-cell communication in the BM and thus control the functioning of the hematopoietic niche, ligand and receptor genes were linked with KEGG (Kyoto Encyclopedia of Genes and Genomes) pathway annotations and filtered to only include interactions where both the ligand and the receptor had the same annotation (Figure 6A). The identified pathways centered around four processes: 1) cell adhesion and migration (including *Cell adhesion molecules CAMS*, *ECM receptor*

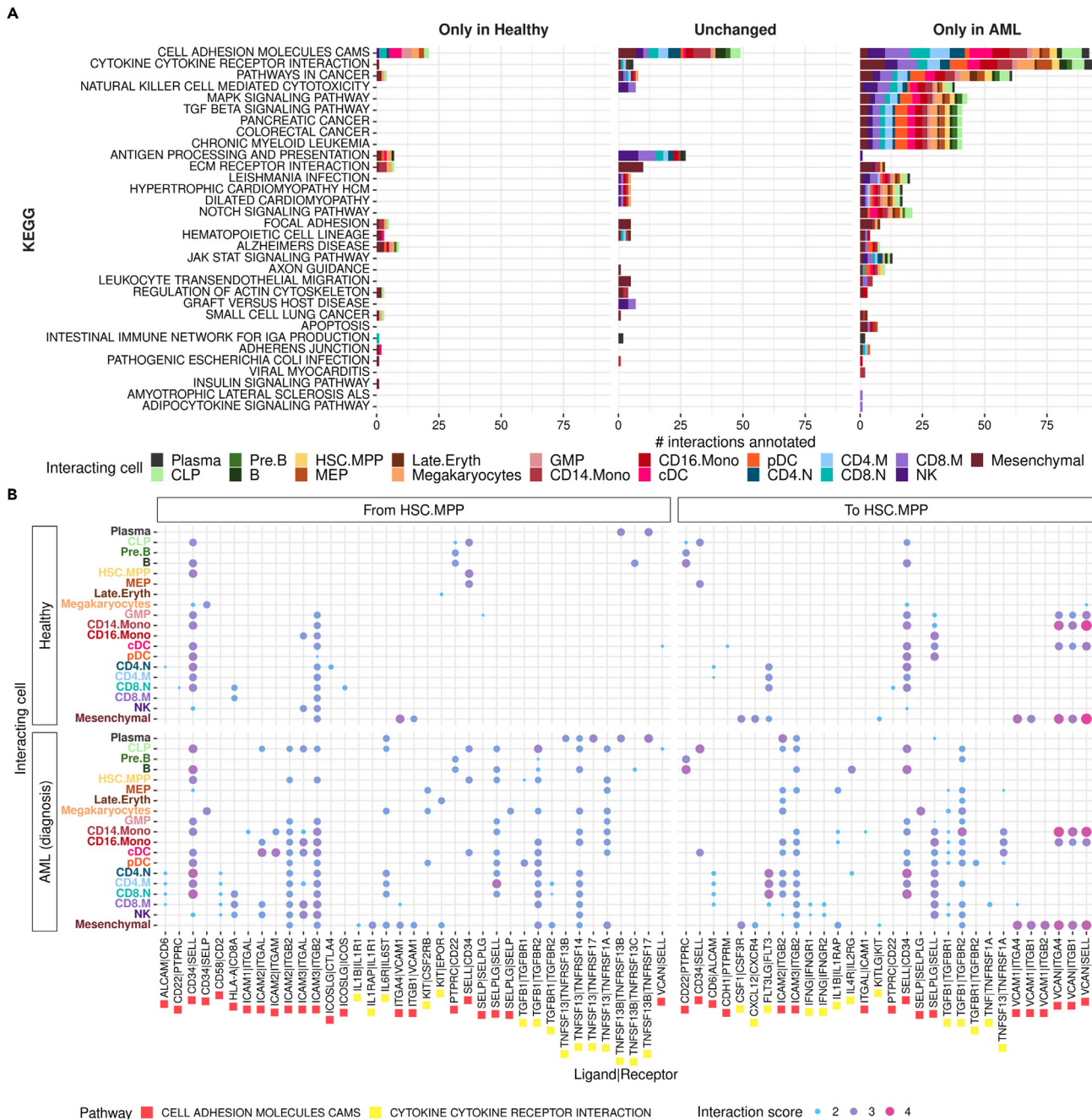


**Figure 6. Altered cell adhesion and cytokine signalling in AML**

(A) Functional annotation of interactions. Predicted interactions were annotated with KEGG pathway annotations and filtered to interactions where the ligand and receptor gene both had the same annotation.

(B) Cell types and signaling molecules involved in interactions annotated with "CELL ADHESION MOLECULES CAMS" or "CYTOKINE CYTOKINE-RECEPTOR INTERACTION". The size and color of each dot represent the interaction score which is a measure of the confidence with which that interaction was identified at a given time point. CD4/8.N, CD4/8 naive T; CD4/8.M, CD4/8 memory T; NK, natural killer cell.

interaction, Focal adhesion, Adherens junction, and Leukocyte transendothelial migration), 2) hematopoiesis and leukocyte maturation (including Hematopoietic cell lineage, NOTCH signaling pathway, and Antigen processing and presentation), 3. cytokine and kinase signaling (Cytokine cytokine receptor interaction, TGF-beta signaling pathway, JAK-STAT signaling pathway, MAPK signaling pathway, Insulin

signaling pathway, and Adipocytokine signaling pathway), and finally 4) cancer-related pathways (including Pathways in cancer, Chronic myeloid leukemia, Colorectal cancer, and Pancreatic cancer) (Figure 6A).

The pathways that the identified ligand-receptor interactions could mediate were restricted and specific to a given cell type/cell lineage in healthy BM (detected only in healthy BM or did not change upon development of AML). Upon development of AML, only a small number of these interactions were lost; instead, an expansion in both the number of possible interactions and participating cell types was detected. Additionally, via newly formed interactions, pathways which were not detected in healthy BM were activated, predominantly regulating cancer-related pathways, cell adhesion, and cytokine signaling (Figure 6A).

To gain insight into the impact of these interactions on HSC.MPP function and the BM microenvironment in AML, the participating ligand-receptor pairs were analyzed for the cell type origin of the signal, the target of the signal if it originated from HSC.MPPs (Figure 6B), and how the predicted interaction changed between healthy and AML BM (Figure 6B). Adhesion of AML cells to the BM niche can confer protection from apoptosis and enhance chemoresistance, and targeting cell adhesion molecules (CAMs) to mobilize malignant cells from the BM has been shown to improve drug sensitivity in AML (e.g., CXCR4 inhibitors).<sup>49</sup> Corroborating this notion, a broad spectrum of interactions mediating cell adhesion were predicted, involving nearly all CAM families, namely the Ig superfamily of CAMs (with members ICAMs, VCAM, ALCAM), integrins (ITGAL [forming LFA-1 when binding to ITGB2], ITGAM [forming Mac-1 with ITGB2], and ITGB2), C-type lectin-like domain proteins (SELL, SELP), and proteoglycans (SELPLG, VCAN) (Figure 6B).

Importantly, cell adhesion interactions between selectin genes (SELL, SELP) and CD34 and the proteoglycan selectin counter-receptor, SELPLG (selectin P ligand/PSGL1), were either upregulated or predicted exclusively in AML samples. SELE is typically expressed by endothelial cells and is known to interact with SELPLG expressed on the surface of leukocytes, including AML blasts. Inhibiting SELE and thus preventing AML cell-endothelium/BM interactions (GMI-1271, uproleselan) has been shown to improve AML patient response to therapy.<sup>50,51</sup> Interestingly, the interactome analysis uncovered another potential selectin interaction not reported in AML before, between SELPLG (expressed by HSC.MPP cells) and SELP (expressed by megakaryocytes, Figure 6B). The therapeutic potential of SELL and SELP in AML is only partially understood but is supported by recent studies in multiple myeloma that showed that platelets can "cloak" malignant cells via SELP to protect them from NK cell-mediated cytotoxicity,<sup>52</sup> and high level of soluble SELL expression has been found to be associated with AML relapse.<sup>53</sup>

HSC.MPPs also participated in numerous potential interactions involving the integrin family, especially the leukocyte integrins, ITGAL, ITGAM, and ITGB2. HSC.MPPs expressed both the integrin ligands, ICAM1-3 and ITGB2, enabling reciprocal interactions between HSC.MPPs and multiple BM-constituent cells. Notably, these predicted interactions substantially expanded in AML. For example, while no interactions were detected for HSPC-expressed ICAM2 in healthy BM, in AML, ICAM2-expressing HSC.MPPs were predicted to form cell-cell interactions with 13 out of the 19 BM cell types expressing ITGB2. Interactions via HSC.MPP-expressed ITGB2, ICAM2, and ICAM3 also became widespread in AML, involving 15 cell types (Figure 6B). This expansion of integrin signaling is likely to play a role in promoting survival of the malignant cells, and although targeting integrins is challenging, these results warrant the study of new, subtype-specific integrin inhibitors for the treatment of AML.<sup>54,55</sup>

With regards to cytokine signaling, a number of novel as well as already known interactions were predicted. One of the most significant of these was IL1B signaling, which has been shown to promote the growth and survival of malignant cells in AML.<sup>29</sup> Ligands and receptors involved in IL1B signaling (IL1B, IL1R1, IL1RAP) were broadly expressed in HSC.MPP cells, monocytes (CD14.Mono, CD16.Mono), and BMSCs (Figure 6B), corroborating the prevailing inflammatory signaling in AML-BM.

The most outstanding novel cytokine pair interactions highlighted by the analysis was TNFSF13 (a proliferation-inducing ligand, APRIL) and TNFSF13B (B cell activating factor of the tumor necrosis factor [TNF] family, BAFF), two key regulators of B cell maturation and survival.<sup>56</sup> TNFSF13B/BAFF is produced by myeloid cells and exerts its effect by binding to three receptors, TNFRSF13B (transmembrane activator and CAML interactor, TACI), TNFRSF13C (BAFF-R), and TNFRSF17 (B cell maturation antigen,

BCMA).<sup>56</sup> Interaction between TNFSF13B and its three receptors was predicted between HSC.MPPs and plasma cells or B cells in healthy BM and was retained in AML. On the other hand, our analysis identified significant upregulation of APRIL in AML in 13 BM cell types, particularly myeloid lineage cells. APRIL, similar to BAFF/TNFSF13B, can also bind to TNFRSF13B and TNFRSF17, while TNFRSF13C is a BAFF-specific receptor. Interaction between TNFSF13/APRIL and its two receptors was predicted in AML-BM corroborating reports that APRIL expression is enhanced in AML cells where it may support leukemic cell proliferation.<sup>57</sup> Underlining the importance of APRIL in malignant transformation, high APRIL expression is also associated with chemoresistance<sup>58</sup> and immunosuppression via facilitating the formation of regulatory B and T cells.<sup>59</sup>

The analysis also predicted that TGFB1 interactions between HSC.MPP and multiple different cell types were present in AML, while TGFB1 interactions were restricted in healthy BM. As mentioned above, widespread TGFB signaling correlated with upregulation of the two TGF- $\beta$  receptors, TGF- $\beta$ -RI (TGFB1, avg. logFC = 1.27, adj. p value = 1.54e-7) and TGF- $\beta$ -RII (TGFB2, avg. logFC = 1.15, adj. p value = 9.75e-9) in AML-HSC.MPPs. TGF- $\beta$  signaling is an important regulator of hematopoiesis and has pleiotropic effects depending on the context.<sup>60</sup> In healthy HSPCs, binding of TGF- $\beta$ 1 to TGF- $\beta$ -R1 and TGF- $\beta$ -R2 represses cell proliferation via induction of the cyclin-dependent kinase inhibitor CDKN1C and other quiescence genes.<sup>61,62</sup> On the other hand, the response of AML HSPCs to TGF- $\beta$ 1 is less well understood.<sup>63</sup> Our data suggest that TGF- $\beta$  signaling is particularly active in AML, and the potential of TGF- $\beta$  signaling as a therapeutic target warrants further research.

### TGFB1 interactions drive stem cell quiescence in AML

Given the increased prevalence of predicted interactions involving TGFB1 in AML and the upregulation of TGFB2 in HSC.MPP cells, we analyzed the downstream consequences of these interactions. Multiple cell types in the niche express TGFB1 (Figure S7) and could contribute to this increased TGFB1 signaling. In the canonical TGF- $\beta$  signaling pathway (Figure 7A), TGF- $\beta$ 1 binds TGF- $\beta$ -R2 leading to the recruitment of TGF- $\beta$ -R1, activation of the Smad transcription factors, SMAD2 and SMAD3, and transcription of target genes, including cyclin-dependent kinase inhibitors, thus inhibiting cell cycling. In healthy HSPCs as well as leukemia stem cells (LSCs)/leukemia-initiating cells, TGF- $\beta$ -R2 activation has been shown to drive quiescence,<sup>4,61,62</sup> which is linked to drug resistance, and new results indicate that inhibition of TGF- $\beta$ -1 signaling may enhance the efficacy of chemotherapy.<sup>64</sup> Given these results, we decided to look for evidence of TGFB1-induced quiescence in AML-HSC.MPPs.

First, activation of TGF- $\beta$ -1 signaling in AML-HSC.MPPs was confirmed by determining the overlap of genes differentially expressed in AML-HSC.MPPs and genes in the canonical TGF- $\beta$ -1 signaling pathway using ingenuity pathway analysis (IPA, Qiagen). TGFB1 was the most significant activated upstream regulator in HSC.MPPs (Figures 7A and 7B). The DEGs also showed presence of a gene signature indicating quiescence in the AML-HSC.MPP population (Figure 7C, gene markers of HSC/LSC quiescence were identified from the literature). Out of a total of 10 genes, 6 were significantly upregulated, indicating enhanced quiescence in the AML-HSC.MPP population in comparison to healthy HSC.MPPs (Figure 7C). Furthermore, we found increased expression of TGFB2 and the LSC quiescence marker, CDKN1A, in AML-HSC.MPPs (Figures 7D and 7E) and a significant positive correlation ( $R = 0.86$ ,  $p < 2.2e-16$ ) between the percentage of CDKN1A+ and TGFB2+ HSC.MPP cells in each sample. This indicates that the increased prevalence of quiescent cells is linked to TGFB1 signaling (Figure 7F). The induction of stem cell quiescence by TGFB1 in AML cells was also assessed in the low-differentiation status (LSC-like) KG1a AML cell line and in primary patient samples. Exposure of KG1a cells to TGF- $\beta$ 1 either as a single agent or in the presence of BM stromal cell co-culture slowed their proliferation (measured with carboxyfluorescein succinimidyl ester [CFSE] dye retention assay). Similarly, TGF- $\beta$ 1 induced the expression of the HSC quiescence markers, CD150 and GPRC5C, in primary, patient-derived AML blasts (Figures 7G, 7H, and 7I). Taken together, these results emphasize the role of TGFB1 in driving AML cell quiescence.

### DISCUSSION

It is well-established that reciprocal interactions between hematopoietic cells and their niche are essential in regulating their properties and functions and that these interactions are skewed in AML generating a microenvironment that fosters leukemogenesis. In this study, we provide several advances by determining the potential interactome of hematopoietic cells in health and AML. By compiling the largest collection of

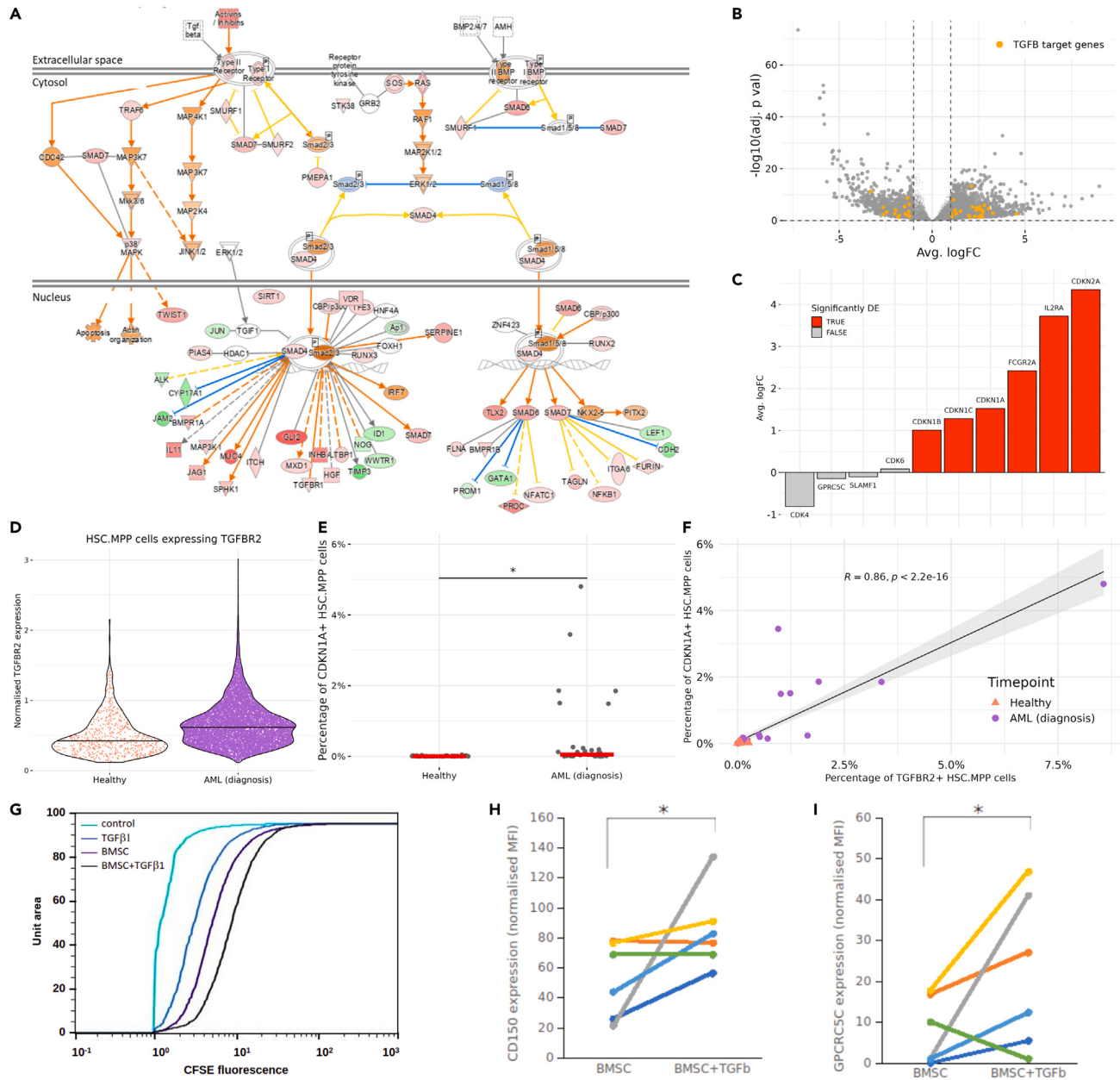


**Figure 7. Interactions involving TGF-β1 drive stem cell quiescence in AML**

- (A) The canonical TGF-β signaling pathway. Red shaded nodes represent genes upregulated in AML. Orange edges represent predicted upregulation/activation based on canonical pathway. Green nodes represent genes downregulated in AML. Blue edges represent predicted downregulation/inhibition based on canonical pathway. Yellow edges represent interactions opposite to prediction.
- (B) Volcano plot showing differential expression of TGF-β1 target genes in HSC.MPP cells in AML.
- (C) Differential expression of genes related to HSC/LSC quiescence in HSC.MPP cells in AML.
- (D) Normalized TGFBR2 expression in HSC.MPP cells (only non-zero values shown).
- (E) Percentage of CDKN1A+ HSC.MPP cells in each sample (CDKN1A+ defined as normalized CDKN1A  $\geq 0.2$ ).
- (F) Correlation between the percentage of CDKN1A+ and TGFBR2+ HSC.MPP cells in each sample (TGFBR2+ defined as normalized TGFBR2  $\geq 0.175$ ).
- (G–I) Proliferation (measured by CFSE fluorescence) of KG1a AML cells cultured alone (control), in the presence of 5 ng/mL transforming growth factor β1 (TGFβ1), bone marrow stromal cell feeder layer (BMSC) or both (BMSC+TGFβ1) for 8 days. Surface expression of CD150 protein H and GPRC5C I determined with immunofluorescence and flow cytometry in primary AML blasts from 5 different donors cultured on BMSC feeder layer either with or without the addition of TGFβ1 for 12 days. \* indicates  $p \leq 0.05$  (student's t-test).

**Table 2. Summary of the publicly available datasets included in this study and where they were obtained from**

Dataset	Downloaded from	Comments
Granja et al. <sup>12</sup>	Data were downloaded in the form of raw count matrices from GEO (GSE139369), and cell metadata was downloaded from the github repository (GreenleafLab/MPAL-Single-Cell2019) accompanying the publication.	Only the samples from healthy donors (BMMC D1T1, BMMC D1T2, CD34 D2T1, CD34 D3T1) were included in this analysis.
Oetjen et al. <sup>13</sup>	Data were downloaded in the form of raw count matrices from GEO (GSE120221).	
Petti et al. <sup>14</sup>	Data were downloaded in the form of raw count matrices from the zenodo link accompanying the publication ( <a href="https://doi.org/10.5281/zenodo.3345981">https://doi.org/10.5281/zenodo.3345981</a> expression_matrices.tar file).	
van Galen et al. <sup>15</sup>	Data were downloaded in the form of raw count matrices from GEO (GSE116256).	The 2 samples from AML cell lines (OCI-AML3 and MUTZ3) were excluded from this analysis.

single-cell gene expression data of the human BM to date, we were able to robustly characterize this complex environment, although it should be noted that certain rare populations of niche cells (e.g., osteoblasts, Schwann cells) are not included in this dataset due to the nature of the samples. Our study leverages several previously generated datasets,<sup>12–15</sup> along with a novel dataset to perform a comprehensive analysis of the hematopoietic niche.

Using this dataset, we determined changes in cell type proportions, cell-type-specific gene expression, and putative cell-cell interactions HSC.MPP form with the other BM-constituent cell types. The results highlight several recurring themes that provide insights into how the microenvironment is corrupted by AML. Firstly, B cell maturation is permanently damaged in AML, shown by the clear decline in the number of CLP and their progeny, including pre.B and B cells, at all AML time points. Unlike T cells, whose numbers partially recover during remission, the significant depletion of B cells persists post-treatment, which likely has implications for the functioning of the adaptive immune system in AML patients even during disease remission. Gene expression changes indicated skewed lymphoid lineage maturation toward T cells rather than B cells and deregulated early B cell maturation, shedding light on the potential reasons for B cell loss in AML.

The predicted HSC.MPP interactions revealed key cell-cell communication pathways that can provide a competitive advantage to AML cells over normal hematopoietic cells including both well-established mechanisms (e.g., CXCL12-CXCR4, FLT3LG-FLT, KITLG-KIT) and several novel ones (SELPLG-SELP, SEMA4D-PLXNB, MIF-CD74, MDK and its receptors, etc). These interactions can drive

1. Enhanced engraftment of AML cells in protective niches, via enhanced cell adhesion mediated via integrins (VLA-5, LFA-1, Mac-1), CD44, and selectins as well as ADAMs
2. Immunosuppression, for example by reduced antigen presentation, and the cytokine, APRIL
3. Impaired BMSC functions/bone resorption via enhanced Notch, TGFB1, and SEMA4D signaling
4. Establishment of an inflammatory environment (IL1B and IL-6)
5. Quiescence of AML cells, mediated by TGF- $\beta$ 1 signaling.

In conclusion, this study provides the first single cell-level characterization of the interactome of HSPCs in the hematopoietic BM niche in health and AML, discovering novel, AML-specific HSPC interactions, and the BM-constituent cell source of these signals at a high granularity. The results reveal the scale of niche alterations that take place in AML and identify promising therapeutic targets to overcome niche-mediated drug resistance.

### Limitations of the study

As mentioned above, one limitation of our study is that the data were generated from BM aspirates which will not have a good representation of cell types such as stromal cells that are more adherent. As such, our

dataset does not include certain rare populations of niche cells (e.g., osteoblasts, Schwann cells) also important to the functioning of the niche. In the future we plan to conduct studies using BM biopsy samples which should have a better representation of all BM cell types. Another limitation is that we are inferring ligand-receptor interactions between cells from gene expression data as surface protein expression is not always reflected at the level of mRNA and it lacks the spatial dimension (adjacency of potentially interacting cells). Nonetheless, many of the predicted interactions are novel and represent potential therapeutic targets to disrupt AML-niche interactions and warrant further investigation and validation.

## STAR★METHODS

Detailed methods are provided in the online version of this paper and include the following:

- [KEY RESOURCES TABLE](#)
- [RESOURCE AVAILABILITY](#)
  - Lead contact
  - Materials availability
  - Data and code availability
- [EXPERIMENTAL MODEL AND STUDY PARTICIPANT DETAILS](#)
  - Bone marrow aspirates and bone marrow stromal cells
  - Cell lines
- [METHOD DETAILS](#)
  - Generation of scRNA-seq dataset
  - Public datasets
  - *In vitro* and *ex vivo* studies
- [QUANTIFICATION AND STATISTICAL ANALYSIS](#)
  - Pre-processing and normalization
  - Batch integration
  - Cell type proportions
  - Differential gene expression
  - Cell-cell interactions

## SUPPLEMENTAL INFORMATION

Supplemental information can be found online at <https://doi.org/10.1016/j.isci.2023.106943>.

## ACKNOWLEDGMENTS

This research was funded by Science Foundation Ireland (SFI) through the SFI Centre for Research Training in Genomics Data Science (18/CRT/6214), the Horizon2020 INTEGRATE MSCA-COFUND programme (H2020-MSCA-COFUND- 945385), Blood Cancer Network Ireland (14-ICS-B3042), DISCOVER-RISE Programme (H2020-RISE-777995), and the Finnish Biobank. We would also like to thank Carsten Riether for his scientific feedback.

## AUTHOR CONTRIBUTIONS

Conceptualization, E.S. and P.Ó.B.; Formal Analysis, S.E. and A.C.; Investigation, E.O.R., S.P.D., T.C., P.N., J.S.T.; Writing – Original Draft, S.E. and E.S.; Writing – Review & Editing, E.S. and P.Ó.B.; Resources, P.N. and P.K.; Supervision, P.K., P.Ó.B., and E.S.

## DECLARATION OF INTERESTS

All authors have reported no financial interests or potential conflicts of interest.

## INCLUSION AND DIVERSITY

We support inclusive, diverse, and equitable conduct of research.

Received: September 19, 2022

Revised: March 22, 2023

Accepted: May 19, 2023

Published: May 23, 2023

## REFERENCES

1. Morrison, S.J., and Scadden, D.T. (2014). The bone marrow niche for hematopoietic stem cells. *Nature* 505, 327–334. <https://doi.org/10.1038/nature12984>.
2. Kokkaliaris, K.D., and Scadden, D.T. (2020). Cell interactions in the bone marrow microenvironment affecting myeloid malignancies. *Blood Adv.* 4, 3795–3803. <https://doi.org/10.1182/bloodadvances.2020002127>.
3. Peled, A., Petit, I., Kollet, O., Magid, M., Ponomaryov, T., Byk, T., Nagler, A., Ben-Hur, H., Many, A., Shultz, L., et al. (1999). Dependence of human stem cell engraftment and repopulation of NOD/SCID mice on CXCR4. *Science* 283, 845–848. <https://doi.org/10.1126/science.283.5403.845>.
4. O'Reilly, E., Zeinabad, H.A., and Szegezdi, E. (2021). Hematopoietic versus leukemic stem cell quiescence: challenges and therapeutic opportunities. *Blood Rev.* 50, 100850. <https://doi.org/10.1016/j.blre.2021.100850>.
5. Krause, D.S., and Scadden, D.T. (2015). A host for the hostile: the bone marrow niche in hematologic neoplasms. *Haematologica* 100, 1376–1387. <https://doi.org/10.3324/haematol.2014.113852>.
6. Duarte, D., Hawkins, E.D., Akinduro, O., Ang, H., De Filippo, K., Kong, I.Y., Haltalli, M., Ruivo, N., Straszkowski, L., Vervoort, S.J., et al. (2018). Inhibition of endosteal vascular remodeling rescues hematopoietic stem cell loss in AML. *Cell Stem Cell* 22, 64–77.e6. <https://doi.org/10.1016/j.stem.2017.11.006>.
7. Oliva, E.N., Franek, J., Patel, D., Zaidi, O., Nehme, S.A., and Almeida, A.M. (2018). The real-world incidence of relapse in acute myeloid leukemia (AML): a systematic literature Review (slr). *Blood* 132, 5188. <https://doi.org/10.1182/blood-2018-99-111839>.
8. Ladikou, E.E., Sivaloganathan, H., Pepper, A., and Chevassut, T. (2020). Acute myeloid leukaemia in its niche: the bone marrow microenvironment in acute myeloid leukaemia. *Curr. Oncol. Rep.* 22, 27. <https://doi.org/10.1007/s11912-020-0885-0>.
9. Baccin, C., Al-Sabah, J., Velten, L., Helbling, P.M., Grünschläger, F., Hernández-Malmierca, P., Nombela-Arrieta, C., Steinmetz, L.M., Trumpp, A., and Haas, S. (2020). Combined single-cell and spatial transcriptomics reveal the molecular, cellular and spatial bone marrow niche organization. *Nat. Cell Biol.* 22, 38–48. <https://doi.org/10.1038/s41556-019-0439-6>.
10. Baryawno, N., Przybylski, D., Kowalczyk, M.S., Kfouri, Y., Severe, N., Gustafsson, K., Kokkaliaris, K.D., Mercier, F., Tabaka, M., Hofree, M., et al. (2019). A cellular taxonomy of the bone marrow stroma in homeostasis and leukemia. *Cell* 177, 1915–1932.e16. <https://doi.org/10.1016/j.cell.2019.04.040>.
11. Stetson, L.C., Balasubramanian, D., Ribeiro, S.P., Stefan, T., Gupta, K., Xu, X., Fourati, S., Roe, A., Jackson, Z., Schauner, R., et al. (2021). Single cell RNA sequencing of AML initiating cells reveals RNA-based evolution during disease progression. *Leukemia* 35, 2799–2812. <https://doi.org/10.1038/s41375-021-01338-7>.
12. Granja, J.M., Klemm, S., McGinnis, L.M., Kathiria, A.S., Mezger, A., Corces, M.R., Parks, B., Gars, E., Liedtke, M., Zheng, G.X.Y., et al. (2019). Single-cell multiomic analysis identifies regulatory programs in mixed-phenotype acute leukemia. *Nat. Biotechnol.* 37, 1458–1465. <https://doi.org/10.1038/s41587-019-0332-7>.
13. Oetjen, K.A., Lindblad, K.E., Goswami, M., Gui, G., Dagur, P.K., Lai, C., Dillon, L.W., McCoy, J.P., and Hourigan, C.S. (2018). Human bone marrow assessment by single-cell RNA sequencing, mass cytometry, and flow cytometry. *JCI Insight* 3, e124928. <https://doi.org/10.1172/jci.insight.124928>.
14. Petti, A.A., Williams, S.R., Miller, C.A., Fiddes, I.T., Srivatsan, S.N., Chen, D.Y., Fronick, C.C., Fulton, R.S., Church, D.M., and Ley, T.J. (2019). A general approach for detecting expressed mutations in AML cells using single cell RNA-sequencing. *Nat. Commun.* 10, 3660. <https://doi.org/10.1038/s41467-019-11591-1>.
15. van Galen, P., Hovestadt, V., Wadsworth Li, M.H., Hughes, T.K., Griffin, G.K., Battaglia, S., Verga, J.A., Stephansky, J., Pastika, T.J., Lombardi Story, J., et al. (2019). Single-cell RNA-seq reveals AML hierarchies relevant to disease progression and immunity. *Cell* 176, 1265–1281.e24. <https://doi.org/10.1016/j.cell.2019.01.031>.
16. Miles, L.A., Bowman, R.L., Merlinsky, T.R., Csete, I.S., Ooi, A., Durruthy-Durruthy, R., Bowman, M., Famulare, C., Patel, M.A., Mendez, P., et al. (2020). Single cell mutational profiling delineates clonal trajectories in myeloid malignancies. *Cancer Biology*. <https://doi.org/10.1101/2020.02.07.938860>.
17. Wang, Z., Li, X., Yang, J., Gong, Y., Zhang, H., Qiu, X., Liu, Y., Zhou, C., Chen, Y., Greenbaum, J., et al. (2021). Single-cell RNA sequencing deconvolutes the *in vivo* heterogeneity of human bone marrow-derived mesenchymal stem cells. *Int. J. Biol. Sci.* 17, 4192–4206. <https://doi.org/10.7150/ijbs.61950>.
18. Triana, S., Vonficht, D., Jopp-Saile, L., Raffel, S., Lutz, R., Leonce, D., Antes, M., Hernández-Malmierca, P., Ordoñez-Rueda, D., Ramas, B., et al. (2021). Single-cell proteo-genomic reference maps of the hematopoietic system enable the purification and massive profiling of precisely defined cell states. *Nat. Immunol.* 22, 1577–1589. <https://doi.org/10.1038/s41590-021-01059-0>.
19. Muschler, G.F., Boehm, C., and Easley, K. (1997). Aspiration to obtain osteoblast progenitor cells from human bone marrow: the influence of aspiration volume. *JBJS* 79, 1699–1709.
20. Lotfollahi, M., Naghipourfar, M., Luecken, M.D., Khajavi, M., Büttner, M., Wagenstetter, M., Avsec, Ž., Gayoso, A., Yosef, N., Interlandi, M., et al. (2022). Mapping single-cell data to reference atlases by transfer learning. *Nat. Biotechnol.* 40, 121–130. <https://doi.org/10.1038/s41587-021-01001-7>.
21. Phipson, B., Sim, C.B., Porrello, E.R., Hewitt, A.W., Powell, J., and Oshlack, A. (2022). propeller: testing for differences in cell type proportions in single cell data. *Bioinformatics* 38, 4720–4726. <https://doi.org/10.1093/bioinformatics/btac582>.
22. Lamble, A.J., Kosaka, Y., Laderas, T., Maffit, A., Kaempf, A., Brady, L.K., Wang, W., Long, N., Saulitz, J.N., Mori, M., et al. (2020). Reversible suppression of T cell function in the bone marrow microenvironment of acute myeloid leukemia. *Proc. Natl. Acad. Sci. USA* 117, 14331–14341. <https://doi.org/10.1073/pnas.1916206117>.
23. Goswami, M., Prince, G., Biancotto, A., Moir, S., Kardava, L., Santich, B.H., Cheung, F., Kotliarov, Y., Chen, J., Shi, R., et al. (2017). Impaired B cell immunity in acute myeloid leukemia patients after chemotherapy. *J. Transl. Med.* 15, 155. <https://doi.org/10.1186/s12967-017-1252-2>.
24. Daver, N., Alotaibi, A.S., Bücklein, V., and Subklewe, M. (2021). T-cell-based immunotherapy of acute myeloid leukemia: current concepts and future developments. *Leukemia* 35, 1843–1863. <https://doi.org/10.1038/s41375-021-01253-x>.
25. Lion, E., Willemen, Y., Berneman, Z.N., Van Tendeloo, V.F.I., and Smits, E.L.J. (2012). Natural killer cell immune escape in acute myeloid leukemia. *Leukemia* 26, 2019–2026. <https://doi.org/10.1038/leu.2012.87>.
26. Squar, J.W., Gautier, M., Kathe, C., Anderson, M.A., James, N.D., Hutson, T.H., Hudelle, R., Qaiser, T., Matson, K.J.E., Barraud, Q., et al. (2021). Confronting false discoveries in single-cell differential expression. *Nat. Commun.* 12, 5692. <https://doi.org/10.1038/s41467-021-2590-2>.
27. Abe, M., Pelus, L.M., Singh, P., Hirade, T., Onishi, C., Purevasuren, J., Taketani, T., Yamaguchi, S., and Fukuda, S. (2016). Internal tandem duplication in FLT3 attenuates proliferation and regulates resistance to the FLT3 inhibitor AC220 by modulating p21Cdkn1a and Pbx1 in hematopoietic cells. *PLoS One* 11, e0158290. <https://doi.org/10.1371/journal.pone.0158290>.
28. Figari, F., Murphy, M.J., Lin, M., and Cleary, M.L. (2008). Pbx1 regulates self-renewal of long-term hematopoietic stem cells by maintaining their quiescence. *Cell Stem Cell* 2, 484–496. <https://doi.org/10.1016/j.stem.2008.03.004>.
29. Carey, A., Edwards, D.K., Eide, C.A., Newell, L., Traer, E., Medeiros, B.C., Polley, D.A., Deininger, M.W., Collins, R.H., Tyner, J.W., et al. (2017). Identification of interleukin-1 by functional screening as a key mediator of cellular expansion and disease progression in acute myeloid leukemia. *Cell Rep.* 18, 3204–3218. <https://doi.org/10.1016/j.celrep.2017.03.018>.

30. Pérez-Vera, P., Reyes-León, A., and Fuentes-Pananá, E.M. (2011). Signaling proteins and transcription factors in normal and malignant early B cell development. *Bone Marrow Res.* 2011, 502751. <https://doi.org/10.1155/2011/502751>.
31. Dimitrov, D., Türei, D., Garrido-Rodriguez, M., Burmedi, P.L., Nagai, J.S., Boys, C., Ramírez Flores, R.O., Kim, H., Szalai, B., Costa, I.G., et al. (2022). Comparison of methods and resources for cell-cell communication inference from single-cell RNA-Seq data. *Nat. Commun.* 13, 3224. <https://doi.org/10.1038/s41467-022-30755-0>.
32. Türei, D., Valdeolivas, A., Gul, L., Palacio-Escat, N., Klein, M., Ivanova, O., Ölbei, M., Gábor, A., Theis, F., Módos, D., et al. (2021). Integrated intra- and intercellular signaling knowledge for multicellular omics analysis. *Mol. Syst. Biol.* 17, e9923. <https://doi.org/10.1525/msb.20209923>.
33. Lee-Thedieck, C., Schertl, P., and Klein, G. (2022). The extracellular matrix of hematopoietic stem cell niches. *Adv. Drug Deliv. Rev.* 181, 114069. <https://doi.org/10.1016/j.addr.2021.114069>.
34. Lagneaux, L., Delforge, A., Dorval, C., Bron, D., and Stryckmans, P. (1993). Excessive production of transforming growth factor- $\beta$  by bone marrow stromal cells in B-cell chronic lymphocytic leukemia inhibits growth of hematopoietic precursors and interleukin-6 production. *Blood* 82, 2379–2385.
35. Terui, T., Niitsu, Y., Mahara, K., Fujisaki, Y., Urushizaki, Y., Mogi, Y., Kohgo, Y., Watanabe, N., Ogura, M., and Saito, H. (1990). The production of transforming growth factor- $\beta$  in acute megakaryoblastic leukemia and its possible implications in myelofibrosis. *Blood* 75, 1540–1548.
36. Matsuda, S., Matsuda, Y., and D'Adamio, L. (2009). CD74 interacts with APP and suppresses the production of A $\beta$ . *Mol. Neurodegener.* 4, 41. <https://doi.org/10.1186/1750-1326-4-41>.
37. Becker-Herman, S., Rozenberg, M., Hillel-Karniel, C., Gil-Yarom, N., Kramer, M.P., Barak, A., Sever, L., David, K., Radomir, L., Lewinsky, H., et al. (2021). CD74 is a regulator of hematopoietic stem cell maintenance. *PLoS Biol.* 19, e3001121. <https://doi.org/10.1371/journal.pbio.3001121>.
38. Christopher, M.J., Petti, A.A., Rettig, M.P., Miller, C.A., Chendamarai, E., Duncavage, E.J., Klco, J.M., Helton, N.M., O'Laughlin, M., Fronick, C.C., et al. (2018). Immune escape of relapsed AML cells after allogeneic transplantation. *N. Engl. J. Med.* 379, 2330–2341. <https://doi.org/10.1056/NEJMoa1808777>.
39. Seyfried, A.N., Maloney, J.M., and MacNamara, K.C. (2020). Macrophages orchestrate hematopoietic programs and regulate HSC function during inflammatory stress. *Front. Immunol.* 11, 1499. <https://doi.org/10.3389/fimmu.2020.01499>.
40. Bonardi, F., Fusetti, F., Deelen, P., van Gosluga, D., Vellenga, E., and Schuringa, J.J. (2013). A proteomics and transcriptomics approach to identify leukemic stem cell (LSC) markers. *Mol. Cell. Proteomics* 12, 626–637. <https://doi.org/10.1074/mcp.M112.021931>.
41. Klein, G., Beck, S., and Müller, C.A. (1993). Tenascin is a cytoadhesive extracellular matrix component of the human hematopoietic microenvironment. *J. Cell Biol.* 123, 1027–1035. <https://doi.org/10.1083/jcb.123.4.1027>.
42. Leng, L., Metz, C.N., Fang, Y., Xu, J., Donnelly, S., Baugh, J., Delohery, T., Chen, Y., Mitchell, R.A., and Bucala, R. (2003). MIF signal transduction initiated by binding to CD74. *J. Exp. Med.* 197, 1467–1476. <https://doi.org/10.1084/jem.20030286>.
43. Varnum-Finney, B., Halasz, L.M., Sun, M., Gridley, T., Radtke, F., and Bernstein, I.D. (2011). Notch2 governs the rate of generation of mouse long- and short-term repopulating stem cells. *J. Clin. Invest.* 121, 1207–1216. <https://doi.org/10.1172/JCI43868>.
44. Azizidoost, S., Bavarsad, M.S., Bavarsad, M.S., Shahrabi, S., Jaseb, K., Rahim, F., Shahjahan, M., Saba, F., Ghorbani, M., and Saki, N. (2015). The role of notch signaling in bone marrow niche. *Hematology* 20, 93–103. <https://doi.org/10.1179/1607845414Y.0000000167>.
45. Takam Kamga, P., Bassi, G., Cassaro, A., Midolo, M., Di Trapani, M., Gatti, A., Carusone, R., Resci, F., Perbellini, O., Gottardi, M., et al. (2016). Notch signalling drives bone marrow stromal cell-mediated chemoresistance in acute myeloid leukemia. *Oncotarget* 7, 21713–21727. <https://doi.org/10.1863/oncotarget.7964>.
46. Pietras, E.M., Mirantes-Barbeito, C., Fong, S., Loeffler, D., Kovtonyuk, L.V., Zhang, S., Lakshminarayanan, R., Chin, C.P., Techner, J.-M., Will, B., et al. (2016). Chronic interleukin-1 exposure drives haematopoietic stem cells towards precocious myeloid differentiation at the expense of self-renewal. *Nat. Cell Biol.* 18, 607–618. <https://doi.org/10.1038/ncb3346>.
47. Arranz, L., Arriero, M.D.M., Villatoro, A., and Villatoro, A. (2017). Interleukin-1 $\beta$  as emerging therapeutic target in hematological malignancies and potentially in their complications. *Blood Rev.* 31, 306–317. <https://doi.org/10.1016/j.blre.2017.05.001>.
48. Geyh, S., Rodríguez-Paredes, M., Jäger, P., Koch, A., Bormann, F., Gutekunst, J., Zilkens, C., Germing, U., Kobbe, G., Lyko, F., et al. (2018). Transforming growth factor  $\beta$ 1-mediated functional inhibition of mesenchymal stromal cells in myelodysplastic syndromes and acute myeloid leukemia. *Haematologica* 103, 1462–1471. <https://doi.org/10.3324/haematol.2017.186734>.
49. Matsunaga, T., Fukai, F., Miura, S., Nakane, Y., Owaki, T., Kodama, H., Tanaka, M., Nagaya, T., Takimoto, R., Takayama, T., and Niitsu, Y. (2008). Combination therapy of an anticancer drug with the FNIII14 peptide of fibronectin effectively overcomes cell adhesion-mediated drug resistance of acute myelogenous leukemia. *Leukemia* 22, 353–360. <https://doi.org/10.1038/sj.leu.2405017>.
50. Barbier, V., Erbani, J., Fiveash, C., Davies, J.M., Tay, J., Tallack, M.R., Lowe, J., Magnani, J.L., Pattabiraman, D.R., Perkins, A.C., et al. (2020). Endothelial E-selectin inhibition improves acute myeloid leukaemia therapy by disrupting vascular niche-mediated chemoresistance. *Nat. Commun.* 11, 2042. <https://doi.org/10.1038/s41467-020-15817-5>.
51. DeAngelo, D.J., Jonas, B.A., Liesveld, J.L., Bixby, D.L., Advani, A.S., Marlton, P., Magnani, J.L., Thackray, H.M., Feldman, E.J., O'Dwyer, M.E., and Becker, P.S. (2022). Phase 1/2 study of uprolecanib added to chemotherapy in patients with relapsed or refractory acute myeloid leukemia. *Blood* 139, 1135–1146. <https://doi.org/10.1182/blood.2021010721>.
52. Henderson, R., Kirkham-McCarthy, L., Swan, D., O'Dwyer, M.E., and Natoni, A. (2018). Platelets preferentially bind to myeloma cells bearing sialofucosylated structures and protect them from natural killer cell-mediated cytotoxicity. *Blood* 132, 4453. <https://doi.org/10.1182/blood-2018-99-116747>.
53. Aref, S., Salama, O., Al-Tonbary, Y., Fouada, M., Menassy, A., and El-Sherbiny, M. (2002). L and E selectins in acute myeloid leukemia: expression, clinical relevance and relation to patient outcome. *Hematology* 7, 83–87. <https://doi.org/10.1080/10245330290028579>.
54. Miller, P.G., Al-Shahrour, F., Hartwell, K.A., Chu, L.P., Järås, M., Puram, R.V., Puissant, A., Callahan, K.P., Ashton, J., McConkey, M.E., et al. (2013). In vivo RNA interference screening identifies a leukemia-specific dependence on integrin beta 3 signaling. *Cancer Cell* 24, 45–58. <https://doi.org/10.1161/j.ccr.2013.05.004>.
55. Oellerich, T., Oellerich, M.F., Engelke, M., Münch, S., Mohr, S., Nimz, M., Hsiao, H.-H., Corso, J., Zhang, J., Bohnenberger, H., et al. (2013).  $\beta$ 2 integrin-derived signals induce cell survival and proliferation of AML blasts by activating a Syk/STAT signaling axis. *Blood* 121, 3889–3899. <https://doi.org/10.1182/blood-2012-09-457887>.
56. Vincent, F.B., Saulep-Easton, D., Figgett, W.A., Fairfax, K.A., and Mackay, F. (2013). The BAFF/APRIL system: emerging functions beyond B cell biology and autoimmunity. *Cytokine Growth Factor Rev.* 24, 203–215. <https://doi.org/10.1016/j.cytogfr.2013.04.003>.
57. Chapellier, M., Peña-Martínez, P., Ramakrishnan, R., Eriksson, M., Talkhoncheh, M.S., Orsmark-Pietras, C., Liljebjörn, H., Höglberg, C., Hagström-Andersson, A., Fioretos, T., et al. (2019). Arrayed molecular barcoding identifies TNFSF13 as a positive regulator of acute myeloid leukemia-initiating cells. *Haematologica* 104, 2006–2016. <https://doi.org/10.3324/haematol.2018.192062>.
58. Bonci, D., Musumeci, M., Coppola, V., Addario, A., Conticello, C., Hahne, M., Gulisano, M., Grignani, F., and De Maria, R. (2008). Blocking the APRIL circuit enhances

- acute myeloid leukemia cell chemosensitivity. *Haematologica* 93, 1899–1902. <https://doi.org/10.3324/haematol.13035>.
59. Tai, Y.-T., Lin, L., Xing, L., Cho, S.-F., Yu, T., Acharya, C., Wen, K., Hsieh, P.A., Dulos, J., van Elsas, A., et al. (2019). APRIL signaling via TACI mediates immunosuppression by T regulatory cells in multiple myeloma: therapeutic implications. *Leukemia* 33, 426–438. <https://doi.org/10.1038/s41375-018-0242-6>.
60. Ruscetti, F.W., Akel, S., and Bartelmez, S.H. (2005). Autocrine transforming growth factor- $\beta$  regulation of hematopoiesis: many outcomes that depend on the context. *Oncogene* 24, 5751–5763. <https://doi.org/10.1038/sj.onc.1208921>.
61. Bataller, A., Montalban-Bravo, G., Soltysiak, K.A., and Garcia-Manero, G. (2019). The role of TGF $\beta$  in hematopoiesis and myeloid disorders. *Leukemia* 33, 1076–1089. <https://doi.org/10.1038/s41375-019-0420-1>.
62. Scandura, J.M., Boccuni, P., Massagué, J., and Nimer, S.D. (2004). Transforming growth factor  $\beta$ -induced cell cycle arrest of human hematopoietic cells requires p57KIP2 up-regulation. *Proc. Natl. Acad. Sci. USA* 101, 15231–15236. <https://doi.org/10.1073/pnas.0406771101>.
63. Dong, M., and Blobel, G.C. (2006). Role of transforming growth factor- $\beta$  in hematologic malignancies. *Blood* 107, 4589–4596. <https://doi.org/10.1182/blood-2005-10-4169>.
64. Tabe, Y., Shi, Y.X., Zeng, Z., Jin, L., Shikami, M., Hatanaka, Y., Miida, T., Hsu, F.J., Andreeff, M., and Konopleva, M. (2013). TGF- $\beta$ -Neutralizing antibody 1D11 enhances cytarabine-induced apoptosis in AML cells in the bone marrow microenvironment. *PLoS One* 8, e62785. <https://doi.org/10.1371/journal.pone.0062785>.
65. Leo, W.J., McLoughlin, A.J., and Malone, D.M. (1990). Effects of sterilization treatments on some properties of alginate solutions and gels. *Biotechnol. Prog.* 6, 51–53. <https://doi.org/10.1021/bp00001a008>.
66. Wolf, F.A., Angerer, P., and Theis, F.J. (2018). SCANPY: large-scale single-cell gene expression data analysis. *Genome Biol.* 19, 15. <https://doi.org/10.1186/s13059-017-1382-0>.
67. Luecken, M.D., and Theis, F.J. (2019). Current best practices in single-cell RNA-seq analysis: a tutorial. *Mol. Syst. Biol.* 15, e8746. <https://doi.org/10.1525/msb.20188746>.
68. Lun, A.T.L., McCarthy, D.J., and Marioni, J.C. (2016). A step-by-step workflow for low-level analysis of single-cell RNA-seq data with Bioconductor. *F1000Res.* 5, 2122. <https://doi.org/10.12688/f1000research.9501.2>.
69. Aran, D., Looney, A.P., Liu, L., Wu, E., Fong, V., Hsu, A., Chak, S., Naikawadi, R.P., Wolters, P.J., Abate, A.R., et al. (2019). Reference-based analysis of lung single-cell sequencing reveals a transitional profibrotic macrophage. *Nat. Immunol.* 20, 163–172. <https://doi.org/10.1038/s41590-018-0276-y>.
70. Wolock, S.L., Lopez, R., and Klein, A.M. (2019). Scrublet: computational identification of cell doublets in single-cell transcriptomic data. *Cell Syst.* 8, 281–291.e9. <https://doi.org/10.1016/j.cels.2018.11.005>.
71. Di Tommaso, P., Chatzou, M., Floden, E.W., Barja, P.P., Palumbo, E., and Notredame, C. (2017). Nextflow enables reproducible computational workflows. *Nat. Biotechnol.* 35, 316–319. <https://doi.org/10.1038/nbt.3820>.
72. Swamy, V.S., Fufa, T.D., Hufnagel, R.B., and McGaughey, D.M. (2021). Building the mega single-cell transcriptome ocular meta-atlas. *GigaScience* 10, giab061. <https://doi.org/10.1093/gigascience/giab061>.
73. Yu, G., Wang, L.-G., Han, Y., and He, Q.-Y. (2012). clusterProfiler: an R Package for comparing biological themes among gene clusters. *OMICS A J. Integr. Biol.* 16, 284–287. <https://doi.org/10.1089/omi.2011.0118>.

## STAR★METHODS

### KEY RESOURCES TABLE

REAGENT or RESOURCE	SOURCE	IDENTIFIER
<b>Antibodies</b>		
Anti-CD150-APC	Miltenyi Biotec	Cat. Number: 130-099-674
Anti-GPRC5C	RnD Systems	Cat. Number: FAB6594G-100UG
<b>Bacterial and virus strains</b>		
NA		
<b>Biological samples</b>		
Bone marrow aspirates	The Finnish Haematology Registry and Clinical Biobank	N/A
<b>Chemicals, peptides, and recombinant proteins</b>		
TGFb1	Pepritech	Cat. Number: 100-21-10ug
CFSE	Biolegend	Cat. Number: 423801
<b>Critical commercial assays</b>		
Chromium Next GEM Single Cell 3' Reagent Kits v3.1	10x Genomics	Product number: PN-1000121
<b>Deposited data</b>		
Raw and processed scRNA-seq data	This paper	GEO: GSE227903
Previously published scRNA-seq data	Granja et al. <sup>12</sup>	GEO: GSE139369
Previously published scRNA-seq data	Oetjen et al. <sup>13</sup>	GEO: GSE120221
Previously published scRNA-seq data	Petti et al. <sup>14</sup>	Zenodo: <a href="https://doi.org/10.5281/zenodo.3345981">https://doi.org/10.5281/zenodo.3345981</a>
Previously published scRNA-seq data	van Galen et al. <sup>15</sup>	GEO: GSE116256
<b>Experimental models: Cell lines</b>		
KG1a cell line	ATCC	Cat. Number: CCL-246.1
<b>Software and algorithms</b>		
R version 4.1	R Core Team	<a href="https://www.r-project.org/">https://www.r-project.org/</a>
R package - scran	Bioconductor	<a href="https://bioconductor.org/packages/release/bioc/html/scran.html">https://bioconductor.org/packages/release/bioc/html/scran.html</a>
R package - SingleR	Bioconductor	<a href="https://bioconductor.org/packages/release/bioc/html/SingleR.html">https://bioconductor.org/packages/release/bioc/html/SingleR.html</a>
R package - scPOP	CRAN	<a href="https://cran.r-project.org/src/contrib/Archive/scPOP/">https://cran.r-project.org/src/contrib/Archive/scPOP/</a>
R package - speckle	Github	<a href="https://github.com/phipsonlab/speckle">https://github.com/phipsonlab/speckle</a>
R package - Libra	Github	<a href="https://github.com/neurorestore/Libra">https://github.com/neurorestore/Libra</a>
R package - clusterProfiler	Bioconductor	<a href="https://bioconductor.org/packages/release/bioc/html/clusterProfiler.html">https://bioconductor.org/packages/release/bioc/html/clusterProfiler.html</a>
R package - liana	Github	<a href="https://github.com/saezlab/liana/">https://github.com/saezlab/liana/</a>
R package - OmnipathR	Bioconductor	<a href="https://www.bioconductor.org/packages/release/bioc/html/OmnipathR.html">https://www.bioconductor.org/packages/release/bioc/html/OmnipathR.html</a>
CellRanger version 6.0.0	10X Genomics	<a href="https://support.10xgenomics.com/single-cell-gene-expression/software/pipelines/latest/installation">https://support.10xgenomics.com/single-cell-gene-expression/software/pipelines/latest/installation</a>
Python version 3.7.4	Python Core Team	<a href="https://www.python.org/">https://www.python.org/</a>

(Continued on next page)

**Continued**

REAGENT or RESOURCE	SOURCE	IDENTIFIER
Python package ScanPy	Github	<a href="https://github.com/scverse/scanpy">https://github.com/scverse/scanpy</a>
Python package scrublet	Github	<a href="https://github.com/swolock/scrublet">https://github.com/swolock/scrublet</a>

**RESOURCE AVAILABILITY****Lead contact**

Further information and requests for resources and reagents should be directed to and will be fulfilled by the lead contact, Eva Szegezdi ([eva.szegezdi@universityofgalway.ie](mailto:eva.szegezdi@universityofgalway.ie)).

**Materials availability**

This study did not generate new unique reagents.

**Data and code availability**

- Raw and processed single-cell RNA-seq data have been deposited at GEO and are publicly available as of the date of publication. Accession numbers are listed in the [key resources table](#). This paper also analyses existing, publicly available data. The accession numbers for these datasets are listed in the [key resources table](#).
- All code needed to reproduce the results in this paper is available on Github ([https://github.com/Sarah145/bone\\_marrow\\_analysis](https://github.com/Sarah145/bone_marrow_analysis)).
- Any additional information required to reanalyse the data reported in this paper is available from the [lead contact](#) upon request.

**EXPERIMENTAL MODEL AND STUDY PARTICIPANT DETAILS****Bone marrow aspirates and bone marrow stromal cells**

The procedure for the sequencing of bone marrow aspirates obtained from The Finnish Haematology Registry and Clinical Biobank was approved by the University of Galway, Research Ethics Committee. Samples were obtained in anonymized form from patients 35–74 years of age. Further information about these samples is available in [Table S2](#). Regarding gender aspects of AML, frequency of AML in males is approximately 1.2– to 1.3-fold higher than in females. To date, there are no correlations known between gender and drug resistance or disease progression. Consequently, both male and female samples were included in all analyses. The ethnicity of the human study participants is unknown. Bone marrow aspirates were collected from AML patients during their routine clinical appointments. After collection, the mononuclear cell fraction was isolated by the Finnish Haematology Registry and Clinical Biobank and provided as a cryopreserved sample for the study.

Primary bone marrow stromal cells (BMSC) were isolated from bone marrow aspirates of AML patients based on their propensity to adhere to plastic. All cells from 2 mL bone marrow aspirate were collected by centrifugation. The cell pellet was resuspended in 5 mL αMEM medium supplemented with 10% HyClone FBS, penicillin (100 U/ml)/streptomycin (100 µg/mL), sodium pyruvate (1 mM), and GlutaMAX (2 mM) and seeded in a T25 flask. After 48 h culture, the non-adhered cells were removed and the adhered BMSCs were expanded.

**Cell lines**

KG1a cells, a promyeloblast cell line derived from the bone marrow of a male AML patient was purchased from ATCC (cat. Number: CCL-246.1). There was no in house authentication carried out.

**METHOD DETAILS****Generation of scRNA-seq dataset**

Longitudinally-collected BM aspirates were obtained for 10 AML patients from the time of diagnosis, post-treatment/remission and at relapse from The Finnish Haematology Registry and Clinical Biobank. The mononuclear cell fraction was isolated using Ficoll density gradient separation. Red cell lysis and dead cell removal (Miltenyi Biotec) was carried out prior to generation of single cell droplets with 10X

Genomics Chromium Controller. Cell counting and viability assessments were conducted using To-Pro3 viability dye. Thereafter, GEM generation & barcoding, reverse transcription, cDNA amplification and 3' gene expression library generation steps were all performed according to the Chromium Next GEM Single Cell 3' Reagent Kits v3.1 (Single Index) User Guide (10x Genomics CG000204 Rev D) with all stipulated 10x Genomics reagents. Generally, 16.5  $\mu$ L of each cell suspension (1,000 cells/ $\mu$ L) and 26.5  $\mu$ L of nuclease-free water were used for a targeted cell recovery of 10,000 cells. GEM generation was followed by a GEM-reverse transcription incubation, a clean-up step and 11 cycles of cDNA amplification. The resulting cDNA was evaluated for quantity and quality using a Thermo Fisher Scientific Qubit 4.0 fluorometer with the Qubit dsDNA HS Assay Kit (Thermo Fisher Scientific, Q32851) and an Advanced Analytical Fragment Analyzer System using a Fragment Analyzer NGS Fragment Kit (Agilent, DNF473), respectively. Thereafter, 3' gene expression libraries were constructed using a sample index PCR step of 14–15 cycles. The generated cDNA libraries were tested for quantity and size using fluorometry and capillary electrophoresis as described above. The cDNA libraries were pooled and sequenced with a loading concentration of 300 p.m., paired end and single indexed, on an illumina NovaSeq 6000 sequencer using a NovaSeq 6000 S1 Reagent Kit v1.5 (100 cycles; illumina, 20028319) and an S4 Reagent Kit v1.5 (200 cycles; illumina, 20028313). The read set-up was as follows: read 1: 28 cycles, i7 index: 8 cycles, i5: 0 cycles and read 2: 91 cycles. The quality of the sequencing runs was assessed using illumina Sequencing Analysis Viewer (illumina version 2.4.7) and all base call files were demultiplexed and converted into FASTQ files using illumina bcl2fastq conversion software v2.20. At least 50,000 reads/cell were generated for each sample. All steps post cell-suspension preparation were performed at the Next Generation Sequencing Platform, University of Bern. Reads were aligned to the GRCh38 reference genome and quantified using CellRanger (version 6.0.0).

### Public datasets

When looking for datasets to include for this analysis, we excluded datasets with fewer than 20,000 genes as we wanted to ensure we captured as much of the transcriptome as possible. [Table 2](#) shows where each dataset was obtained from.

### In vitro and ex vivo studies

#### Reagents

All materials were purchased from Sigma-Aldrich unless stated otherwise. 2% sodium alginate was prepared by dissolving sodium alginate in phosphate buffered saline (PBS) and sterilized by heating to 80°C in a water bath for 15 min.<sup>65</sup> Carboxyfluorescein succinimidyl ester (CFSE) (Biolegend) was dissolved in dimethyl sulfoxide (DMSO). Annexin V-APC was purchased from Immunotools. Anti-CD150PE and anti-GRPC5C Alexa Fluor 405 antibodies were purchased from R&D Systems. TGF- $\beta$ 1 was obtained from Peprotech.

#### Cell culture

KG1a cells were maintained at a density of 500,000 cells/ml in RPMI-1640 supplemented with GlutaMAX (Gibco, 2 mM), 10% HyClone fetal bovine serum (FBS, Thermo Fisher Scientific), penicillin (100 U/ml), streptomycin (100  $\mu$ g/mL) and sodium pyruvate (1 mM). Bone marrow mesenchymal stromal cells (BMSCs; hTERT immortalized primary BMSCs from a healthy donor) were cultured at a density of 50,000 cells/ml in  $\alpha$ MEM (Sigma-Aldrich) supplemented with 10% HyClone FBS, penicillin (100 U/ml)/streptomycin (100  $\mu$ g/mL), sodium pyruvate (1 mM) and GlutaMAX (2 mM).

#### Primary AML blast samples

Mononuclear cell fractions generated from bone marrow aspirates were obtained from Blood Cancer Biobank Ireland. All patients provided written informed consent. For BMSC-AML co-cultures, BMSCs were re-suspended in 2% alginate solution at 500,000 cells/ml and aliquoted in 24-well plates (200  $\mu$ L/well). The alginate was crosslinked by addition of 100 mM CaCl<sub>2</sub> for 10 s, forming a layer of BMSCs trapped in the alginate scaffold. Excess CaCl<sub>2</sub> was removed by three washes with DPBS (Gibco). KG1a cells and primary AML blasts at  $5 \times 10^6$  cells/ml density were labeled with the long-term cell tracker, carboxyfluorescein diacetate succinimidyl ester (CFSE, Biolegend, 2.5  $\mu$ M) as per manufacturers instructions. The cells were resuspended in IMDM growth medium (supplemented with 10% HyClone fetal bovine serum (FBS, Thermo Fisher Scientific), penicillin (100 U/ml), streptomycin (100  $\mu$ g/mL) and sodium pyruvate (1 mM) and seeded

on top of the alginate trapped BMSCs with or without TGF- $\beta$ 1 (5 ng/mL) at 50,000 cells/ml for KG1a cells and at 500,000 cells/ml for primary AML samples.

#### Immunofluorescence, cell cycle and viability analysis

Dye retention was analyzed by detecting CFSE fluorescence intensity in the live cell fraction. Viability was determined using Annexin V-APC staining. KG1a cells previously labeled with CFSE were collected from single cultures by pipetting. From cocultures, in addition to pipetting off the suspension cells, 200  $\mu$ L of 1 mM ethylenediaminetetraacetic acid (EDTA) was also added to loosen the alginate. The cells were pelleted and resuspended in Annexin V buffer (10 mM HEPES/NaOH, pH 7.5, 140 mM NaCl, 2.5 mM CaCl<sub>2</sub>) containing 1.5  $\mu$ L Annexin V-APC (ImmunoTools). The cells were incubated on ice in the dark for 15 min, followed by analysis by flow cytometry. The intensity of the CFSE signal was measured in the live cell fraction as a determinant of cell proliferation rate. For immunofluorescence labeling, primary AML blasts were harvested and resuspended in 1% bovine serum albumin (BSA) in PBS and blocked for 10 min after which the cells were collected and resuspended in 100  $\mu$ L 1% BSA/PBS containing 2  $\mu$ L of antibodies SLAMF1/CD150-PE (R&D Systems) or GRPC5C Alexa Fluor 405 (R&D Systems) and incubated on ice in the dark for 30 min. After washing of unbound antibodies with 400  $\mu$ L of 1% BSA/PBS, the cells were resuspended in 200  $\mu$ L of 1% BSA/PBS for measurement.

## QUANTIFICATION AND STATISTICAL ANALYSIS

#### Pre-processing and normalization

Datasets were analyzed using a uniform pre-processing pipeline to ensure consistency. In the case where cell quality control needed to be performed, this was done using the ScanPy python module<sup>66</sup> according to current best-practices.<sup>67</sup> Counts were normalized using the computeSumFactors function from the scran R package.<sup>68</sup> The SingleR R package<sup>69</sup> was used to predict cell type labels for each dataset using the Granja et al.<sup>12</sup> dataset as a reference. This dataset was chosen as the reference dataset as it is a CITE-seq dataset with expression values for several cell surface proteins and so the cell type labels should be reliable. Doubts were identified using Scrublet<sup>70</sup> and removed. All datasets were then merged into a single matrix for batch correction.

#### Batch integration

Batch correction was performed using scArches<sup>20</sup> (2000 highly variable genes, 20 latent dimensions) and a nearest neighbor graph was constructed from the latent dimensions (n neighbors = 15) to generate a UMAP graph. The integrated UMAP graph showed good mixing of cells from different datasets, indicating that the datasets are well integrated (Figure S5). A NextFlow<sup>71</sup> pipeline was developed to test different values for number of highly variable genes, latent dimensions and neighbors, to determine which values would yield the optimal integration results using the scPOP R package<sup>72</sup> to evaluate the results on the basis of Adjusted Rand Index (ARI), Normalized Mutual Information, Silhouette Width and Local Inverse Simpson Index (LISI). The results are shown in Table S2.

#### Cell type proportions

The propeller function from the speckle R package was used to test whether there are statistically significant changes in cell type proportions between the different conditions.<sup>21</sup> Samples that were sorted prior to sequencing (n = 6) were excluded from this analysis.

#### Differential gene expression

For each cell type, differentially expressed genes were identified by comparing gene expression in healthy samples to gene expression in AML (diagnosis) samples. To avoid calling too many false positives, the Libra R package<sup>26</sup> was used to implement a pseudobulk approach to calculate differential expression and genes with absolute average log fold change  $\geq 1$  and an adjusted p value  $\leq 0.05$  were labeled differentially expressed. The DEG analysis was performed on the uncorrected gene expression values (pre-integration) but a batch label was included in the model to account for batch effects between datasets. Figure S6 shows that there is no consistent batch effect obvious for the top DEGs, i.e. no one dataset appears to be driving the differential expression results. Significant DEGs for each cell type were used as input for a Gene Ontology enrichment analysis using the clusterProfiler R package.<sup>73</sup>

**Cell-cell interactions**

For the prediction of cell-cell interactions, healthy and diagnosis samples were isolated from the larger dataset and 1000 cells (or all cells if  $n \leq 1000$ ) of each cell type were subsampled. The liana R package<sup>31</sup> was used to run 5 different methods for predicting cell-cell interactions (cellphonedb (squidpy), cellchat, NATMI, iTALK and SingleCellSignalR) using the Omnipath database resource of ligand-receptor interactions.<sup>32</sup> Results were filtered to interactions where either HSC.MPP cells were expressing either the ligand or receptor gene. To avoid calling false positive interactions, only interactions with curation effort  $\geq 3$  were considered. The liana\_aggregate function was used to generate an aggregate rank score for each interaction and interactions with a score  $\leq 0.05$  were considered to be high-confidence interactions. The OmnipathR R package was used to import functional annotations (KEGG and CellChat) for all genes involved in ligand-receptor interactions.<sup>32</sup>